CHALMERS

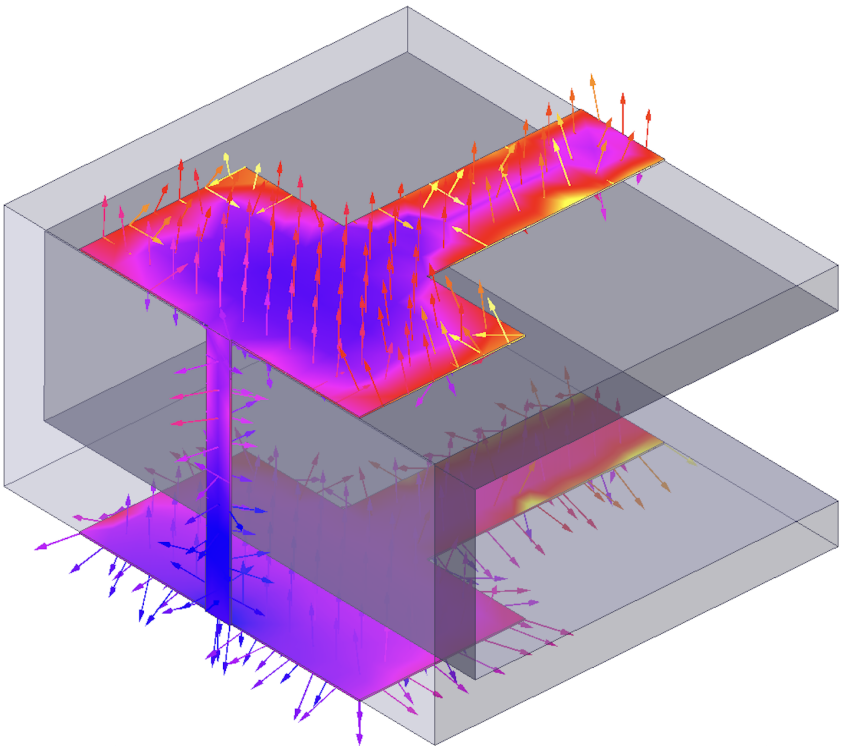

Design and Performance Analysis of 2D and 3D Microwave Filters Using Additive Manufacturing Techniques

Focusing on Chebyshev Low-Pass Filter Implementations

Bachelor's Thesis in Electrical Engineering

Isabella Arnesson

Department of Microtechnology and Nanoscience
CHALMERS UNIVERSITY OF TECHNOLOGY
Gothenburg, Sweden 2026
www.chalmers.se

Degree project report 2026

Design and Performance Analysis of 2D and 3D Microwave Filters Using Additive Manufacturing Techniques

Focusing on Chebyshev Low-Pass Filter Implementations

Isabella Arnesson

CHALMERS
UNIVERSITY OF TECHNOLOGY

Department of Microtechnology and Nanoscience
Chalmers University of Technology
Gothenburg, Sweden 2026

Design and Performance Analysis of 2D and 3D Microwave Filters Using Additive Manufacturing Techniques
Focusing on Chebyshev Low-Pass Filter Implementations
Isabella Arnesson

Supervisor: Andreas DivinyiName, Saab Surveillance,
Supervisor: Lukas Mared, Saab Surveillance
Supervisor: Vessen Vassilev, Monolithic Microwave Integrated Circuits

Examiner: Vessen Vassilev, Monolithic Microwave Integrated Circuits

Degree project report 2026
Department of Microtechnology and Nanoscience
Chalmers University of Technology
SE-412 96 Gothenburg
Sweden
Telephone +46 31 772 1000

Cover: Electric field distribution of a three-dimensional microwave filter structure, simulated in ANSYS HFSS. The visualization shows the field vectors across multiple substrate layers.

Typeset in LaTeX
Gothenburg, Sweden 2026

Design and Performance Analysis of 2D and 3D Microwave Filters Using Additive Manufacturing Techniques
Focusing on Chebyshev Low-Pass Filter Implementations
Isabella Arnesson
Department of Microtechnology and Nanoscience
Chalmers University of Technology

Abstract

This thesis investigates whether three-dimensional microwave filter structures, enabled by inkjet-based additively manufactured electronics (AME), can improve performance or reduce the physical size of microwave filters compared to conventional two-dimensional designs. A third-order Chebyshev low-pass filter was implemented as the reference design in ANSYS HFSS and compared against six three-dimensional configurations, including modified ground plane structures, multi-level conductor arrangements, and geometrical variations of the signal path. The performance of each configuration was evaluated using S-parameters and electric field distributions.
The results show that ground plane placement proved decisive for filter behavior across all tested configurations. Three-dimensional modifications can preserve acceptable low-pass filter performance, but only when the return current path remains controlled and transitions between filter sections are kept smooth. Among the investigated configurations, the most compact designs achieve reductions in planar footprint down to 28% and 32% of the reference, respectively, at the cost of modified frequency responses, while the most geometrically controlled three-dimensional structure maintains a cutoff frequency closely comparable to the reference filter. What matters is not simply adding a third dimension, but understanding and controlling what happens electromagnetically when you do.

Keywords: Microwave filters, microstrip, three-dimensional structures, additive manufacturing, S-parameters, Chebyshev filter, HFSS, AME.

Acknowledgements

I would like to thank my supervisors Lukas Mared and Andreas Divinyi at Saab Surveillance, for their support throughout this project. Lukas Mared provided valuable guidance on how to navigate the simulation software and provided detailed feedback on the report. Andreas Divinyi contributed with feedback on how to structure and approach the work, as well as constructive comments on the report throughout the project. The authors also thank my supervisor and examiner at Chalmers University of Technology, Vessen Vassilev, for ensuring that the work maintained an academic standard and for valuable feedback during the course of the project.

Isabella Arnesson, Gothenburg, May 2026

Contents

List of Figures

List of Tables

1

Introduction

This chapter provides background and motivation for the study of three-dimensional microwave filter design enabled by additive manufacturing, followed by a description of the purpose and method. The research questions are then stated, and the chapter ends with a discussion of the limitations of the work.

1.1 Background

The development of additive manufacturing technologies has opened up new possibilities for the design and fabrication of microwave components. In particular, additively manufactured electronics (AME) based on multi-material inkjet printing enables the simultaneous deposition of conductive and dielectric materials in a single process. This makes it possible to realize complex three-dimensional structures with conductors and dielectric regions distributed at different vertical levels, including multilayer circuit boards with vias [1]. This differs fundamentally from conventional printed circuit board (PCB) based implementations, where the design is restricted to planar conductive layers separated by dielectric substrates.

In high-frequency systems, filters are widely used in applications such as wireless communications, radar, and sensing, where precise control of the frequency spectrum is required [2]. Traditionally, such filters are implemented using planar PCB technologies, which limit the design flexibility and the possibility of exploiting three-dimensional electromagnetic effects. An example of a conventional planar microwave PCB implementation is shown in Fig. 1.1. The design freedom enabled by AME is therefore particularly relevant for microwave filter design, since the geometry of the conductor and ground structure directly determine the electromagnetic behavior of the filter.

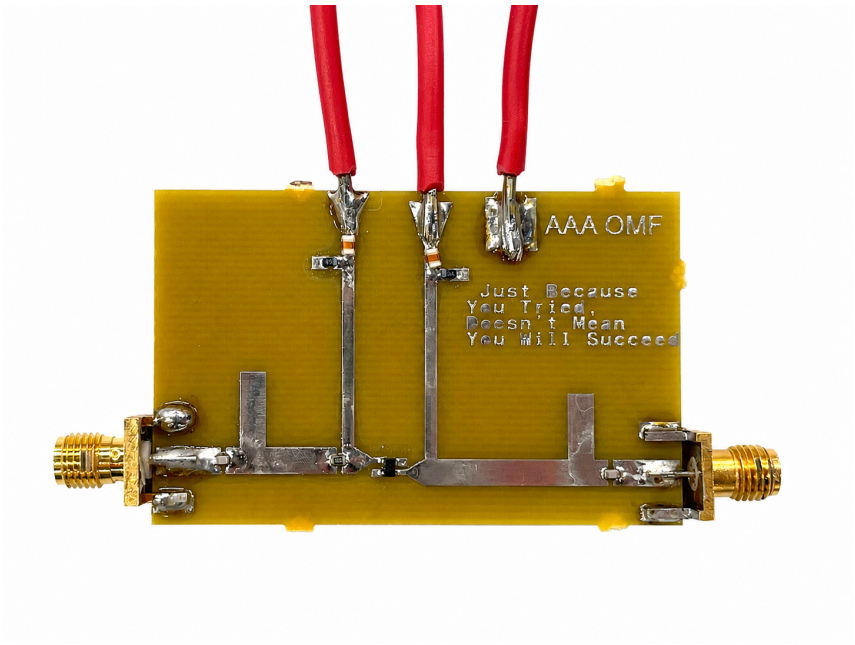

Figure 1.1: Example of a conventional planar microwave PCB filter. The filter was fabricated by the author in a previous course project and is used here as a visual example of planar microwave PCB technology.

In compact microwave systems such as phased-array and active electronically scanned array (AESA) radar applications, filter size is often an important design consideration. These systems can contain a large number of radio frequency (RF) components that must be integrated within a limited volume, making a reduced planar footprint relevant for system integration. More generally, microwave hardware is often evaluated in terms of size, weight, power, and cost (SWaP-C), where physical size is an important factor for compact system design.

The capabilities of AME technology have been demonstrated in several microwave applications. A multimetal layer bandpass filter fabricated using low-temperature inkjet printing showed good agreement between simulated and measured results while achieving miniaturization through vertically integrated inductive and capacitive structures [3]. Planar capacitors manufactured directly as part of an electronic circuit board using AME demonstrate superior RF performance compared to conventional surface-mount components, with lower parasitic inductance and resistance due to the elimination of soldering and external packaging [4]. Together, these results suggest that AME is mature enough to warrant a more systematic look at its use in microwave filter design.

No study yet compares conventional planar filter designs, where all conductive elements lie on a single horizontal surface, with 3D implementations where parts of the filter structure extend into the vertical dimension, under the same simulation conditions. Prior work has shown that AME-fabricated filters can be built, but not what 3D geometry alone does to performance. This thesis addresses that gap by investigating what 3D geometry does to filter performance, rather than fabricating a physical component.

1.2 Purpose and Method

To address the identified gap, the purpose of this thesis is to investigate whether 3D microwave filter structures, conceptually enabled by the design freedom of additive manufacturing technologies such as AME, can improve the performance or reduce the physical size of microwave filters compared to conventional 2D designs.

The study is conducted through full-wave electromagnetic simulations in ANSYS HFSS. A 2D reference filter is first designed and then used as the basis for a series of 3D configurations. These geometries represent structures that are conceptually made possible by AME-based fabrication, allowing conductors, dielectric regions, and ground structures to be distributed in three dimensions. This type of geometric freedom is difficult or impractical to achieve with conventional planar PCB processes. The configurations investigated include modifications to the ground plane, multi-level conductor structures, and geometrical variations that make use of the third dimension in different ways. The performance of each design is evaluated in terms of insertion loss, return loss, cutoff frequency, and physical size, allowing a direct comparison between planar and 3D implementations.

All configurations share the same starting point: a third-order Chebyshev low-pass filter chosen for its well-defined theoretical response. This filter type is well-suited for comparative analysis, as it has a well-defined theoretical foundation and a predictable frequency response based on classical filter theory [2]. A third-order filter provides a sufficiently simple structure for controlled geometrical modifications while still exhibiting a representative low-pass filter response with both inductive and capacitive sections. This provides a practical and controlled basis for evaluating how 3D modifications affect the filter behavior.

The goal is to identify which 3D geometries are worth pursuing further and which introduce problems that outweigh any size benefit.

1.3 Research Questions

The main research question of this thesis is:

- Can 3D microwave filter geometries, conceptually enabled by the design freedom of additive manufacturing, improve performance or reduce the physical size compared to conventional 2D designs?

To address this, the following sub-questions are investigated:

- How do selected 3D geometrical modifications affect insertion loss, return loss, bandwidth, cutoff frequency, and physical size?
- How do these geometrical modifications affect the electromagnetic field distribution and impedance behavior of the filter?
- What trade-offs arise between filter performance, miniaturization, and geometrical complexity when extending microwave filter designs into three dimensions?

1.4 Limitations

The scope of this study is subject to several limitations that should be considered when interpreting the results.

The investigated geometries are conceptually designed with the design freedom of additive manufacturing in mind, where conductors, dielectric regions, and ground structures can be distributed in three dimensions. However, the models are not optimized for a specific additive manufacturing process, and process-specific constraints such as minimum feature size, print resolution, layer alignment, and manufacturability are not evaluated in detail.

All results come from HFSS simulations, and no physical filters were built or measured as part of this work. As a result, fabrication constraints and manufacturing-related effects are not evaluated. This includes fabrication tolerances, surface roughness, material inconsistencies, minimum feature size, print resolution, and layer alignment. Material parameters such as the dielectric constant and the loss tangent are treated as constant throughout the study, which can lead to discrepancies between the simulated and real-world performance at higher frequencies [1].

In this study, the dielectric constant and the loss tangent are treated as constant, which is a common simplification in simulation-based studies but introduces some error at higher frequencies where frequency-dependent material behavior can become significant.

Only configurations derived from a third-order Chebyshev low-pass filter are studied. The simulation range spans 5 to 20 GHz, chosen to cover both the passband and stopband of the reference filter while ensuring that the -3 dB cutoff frequency can be identified for all investigated configurations. The lower bound of 5 GHz reflects that the stepped-impedance microstrip implementation does not produce a meaningful filter response at very low frequencies.

The conclusions may therefore not be directly generalizable to other filter types, higher-order designs, or different frequency ranges.

The aim of this work is not to maximize the performance of any individual design but rather to evaluate the feasibility and electromagnetic behavior of different 3D configurations in comparison to the 2D reference. Differences in performance should therefore be interpreted in this context.

The analysis is further limited to S-parameter responses and electric field distributions as the primary evaluation tools. In this work, other performance metrics such as the unloaded quality factor, the current density distribution, and the conductor losses are not evaluated. Since none of the investigated models are optimized and the primary focus is on comparing the low-pass behavior and electromagnetic field confinement across different 3D configurations, these metrics are considered outside the scope of the present study. They represent relevant directions for future work, particularly when optimizing specific filter configurations for practical implementation.

Certain electromagnetic effects observed in the simulations, such as resonances introduced by vertically distributed conductor structures or modified ground plane configurations, may also be influenced by modeling choices such as boundary conditions, port definitions, and meshing strategies. These effects may behave differently

in physical implementations and should be interpreted with appropriate caution. Finally, the study does not include a complete SWaP-C analysis. The weight, power handling, manufacturing cost, and process-specific limitations associated with additive manufacturing are outside the scope of this work, and these factors may play a significant role in determining the practical feasibility of the proposed designs.

2

Theory

This chapter introduces the theoretical background needed to understand the design choices, simulation results, and comparisons presented in the following chapters. First, microwave filters and S-parameters are introduced as the basis for evaluating filter behavior. Microstrip technology and PCB stacking concepts are then described to provide context for the investigated filter geometries. Finally, low-pass filter theory is presented with focus on the Chebyshev approximation and stepped-impedance implementation is presented, followed by a discussion of 3D filter concepts in relation to additive manufacturing.

2.1 Microwave Filters

Filters are fundamental components in electronic systems that are used to selectively pass or reject signals depending on their frequency. In their most general form, filters can be described using lumped reactive elements such as inductors and capacitors, and are commonly categorized according to their frequency response as low-pass, high-pass, band-pass or band-stop filters [2]. The ideal frequency response of each filter type is defined by its passband, where signals pass with minimal attenuation, its stopband, where signals are strongly attenuated, and the transition band between them.

Microwave filters are essential components in high-frequency systems, where they are used to selectively pass or reject specific frequency components of an electromagnetic signal. The microwave frequency range is generally considered to range from approximately 300 MHz to 300 GHz [2]. Within this range, filters are commonly used in systems such as wireless communications, radar, and sensing, where precise control of the frequency spectrum is required.

Filters are commonly categorized into low-pass, high-pass, band-pass, and band-stop filters, depending on which frequency ranges they allow to propagate. The frequency response of a filter is described in terms of three regions: the passband, where signals pass with minimal attenuation; the stopband, where signals are strongly attenuated; and the transition band between them. The width of the transition band and the attenuation in the stopband depend on the filter order and the chosen approximation [2]. Figure 2.1 illustrates these regions for a schematic low-pass filter response.

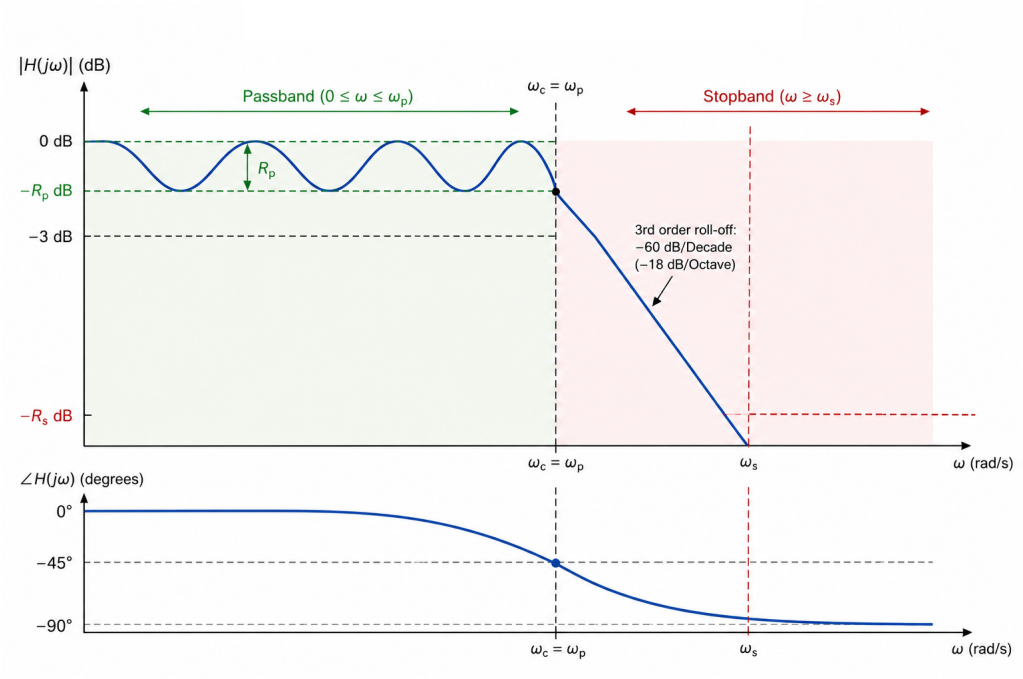

Figure 2.1: Schematic low-pass filter response showing the passband, transition band, stopband, and cutoff frequency.

At microwave frequencies, the physical dimensions of circuit elements can become comparable to the wavelength of the signals. As a result, microwave filters are often implemented using distributed elements, such as transmission lines, rather than ideal lumped inductors and capacitors. The filter approximation and implementation used in this work are described in Section 2.5.

2.2 Scattering parameters

Scattering parameters (S-parameters) are a set of parameters used to describe the electrical behavior of microwave networks in terms of incident and reflected power waves. Filter performance is evaluated through the S-parameters, specifically S_{11} and S_{21}. For a two-port network such as a filter, the most important parameters are the input reflection coefficient S_{11} and the forward transmission coefficient S_{21}.

The parameter S_{11} describes how much of the signal incident at port 1 is reflected back toward the source, and is therefore used to evaluate the input matching of the filter. A low value of S_{11} indicates that only a small part of the incident signal is reflected. The parameter S_{21} describes how much of the signal incident at port 1 is transmitted to port 2 and is therefore used to evaluate insertion loss, cutoff behavior, and stopband attenuation. Figure 2.2 illustrates the basic meaning of these parameters for a two-port network.

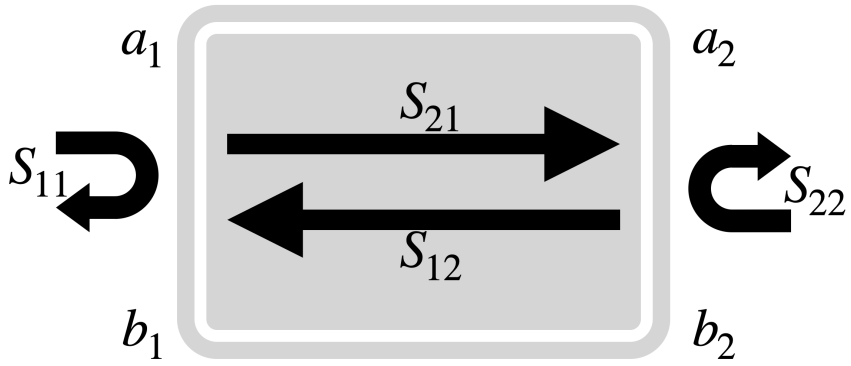

Figure 2.2: Conceptual illustration of S-parameters for a two-port network. The incident waves are denoted by a_1 and a_2, and the outgoing waves by b_1 and b_2.

In the S-parameter formulation introduced by Kurokawa [5], microwave networks are described in terms of incident and reflected power waves rather than directly in terms of voltages and currents. The incident waves a_1 and a_2 represent signals entering the two ports, while the outgoing waves b_1 and b_2 represent signals leaving the ports. For a two-port network, the relationship between these waves can be written as follows

$$\begin{pmatrix} b_1 \\ b_2 \end{pmatrix} = \begin{pmatrix} S_{11} & S_{12} \\ S_{21} & S_{22} \end{pmatrix} \begin{pmatrix} a_1 \\ a_2 \end{pmatrix}. \tag{2.1}$$

In this matrix, S_{11} describes reflection at port 1, S_{21} describes transmission from port 1 to port 2, S_{12} describes reverse transmission from port 2 to port 1, and S_{22} describes reflection at port 2. In this work, only S_{11} and S_{21} are evaluated, since filter performance is assessed from input reflection and forward transmission.
A general S-parameter can be defined as

$$S_{ij} = \left.\frac{b_i}{a_j}\right|_{a_k=0 \text{ for } k\neq j} \tag{2.2}$$

where a_j is the incident wave in port j and b_i is the outgoing wave in port i. The S-parameters are commonly expressed in decibels as $20\log_{10}(|S_{ij}|)$. The equations are included to define the quantities used in the analysis, but the numerical values used in this work are obtained directly from the HFSS simulations.

2.3 Microstrip Technology

Microstrip technology is one of the most widely used methods for implementing microwave circuits on printed circuit boards. A microstrip structure consists of a conductive strip placed on top of a dielectric substrate, with a continuous ground plane on the opposite side, as illustrated in Figure 2.3.

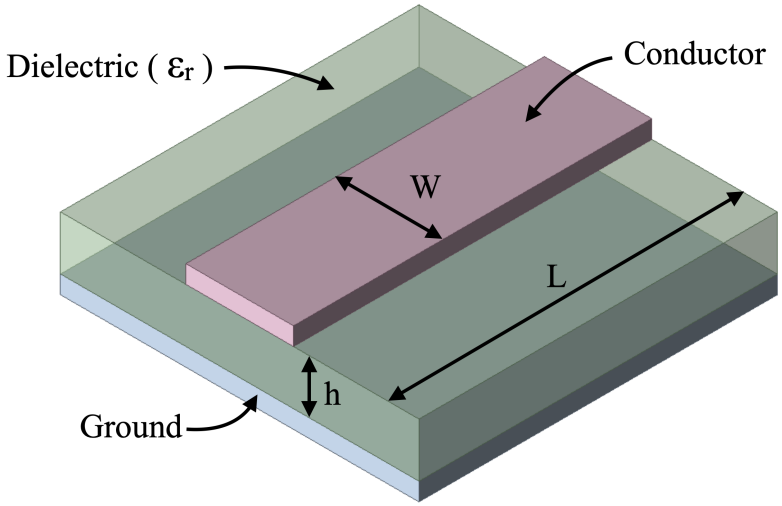

Figure 2.3: Cross-sectional representation of a microstrip transmission line showing the conductor width (W), substrate thickness (h), dielectric constant (ε_r), and ground plane.

In contrast to ideal transmission lines, the electromagnetic fields in a microstrip are not fully confined within the dielectric material. Instead, the fields are distributed partly in the substrate and partly in the air above the conductor. A pure transverse electromagnetic (TEM) mode has electric and magnetic fields that are entirely transverse to the direction of propagation. Because the fields in a microstrip extend through both dielectric material and air, the structure supports a quasi-TEM mode, meaning that the field behavior is close to TEM but not ideal. As a result, the effective permittivity ε_{eff} is determined by both the substrate permittivity and the permittivity of the surrounding air [2]. The effective permittivity can be approximated as

$$\varepsilon_{\text{eff}} = \frac{\varepsilon_r + 1}{2} + \frac{\varepsilon_r - 1}{2} \frac{1}{\sqrt{1 + 12h/W}} \tag{2.3}$$

where ε_r is the relative permittivity of the substrate, h is the thickness of the substrate, and W is the width of the conductor [2].

Because the fields spread through both substrate and the air, fringing effects alter the effective electrical length and introduce parasitics that grow more significantly at higher frequencies.

The characteristic impedance of a microstrip line depends primarily on the conductor width and the substrate properties, but is also influenced by factors such as conductor thickness, ground plane geometry, and surrounding materials. By adjusting the conductor width, different characteristic impedances can be realized within the same substrate. This property is the basis for implementing distributed filter structures, such as the stepped-impedance low-pass filter used in this work.

2.4 PCB Stack-Up and Multi-Level Structures

In conventional PCB technology, the conductive layers are separated by dielectric material and arranged within a predefined stack-up. The term stack-up refers to the order and thickness of the conductive and dielectric layers in the PCB structure. In a standard multilayer PCB, the conductor layers are planar, and the vertical arrangement is mainly used to route signals between layers through vertical interconnections known as vias (plated through holes, PTH).
In this thesis, the term multi-level structure is used to describe filter geometries where parts of the signal path or ground configuration are intentionally placed at different vertical positions. This is distinct from a conventional multilayer PCB, where the vertical arrangement is used primarily for signal routing rather than as a geometrical design variable. The multi-level structures investigated in this work are conceptually enabled by the design freedom of additive manufacturing, where conductors and dielectric regions can be distributed more freely in three dimensions than what is possible with conventional PCB processes.

2.5 Low-Pass Filter Theory

Low-pass filters are designed to pass signals below a specified cutoff frequency with minimal attenuation while attenuating signals at higher frequencies. The transition between the passband and the stopband is determined by the filter order and the chosen approximation [2].
A classical low-pass filter can be represented using lumped reactive elements such as inductors and capacitors. In a third-order low-pass filter, the equivalent lumped-element circuit takes the form of a C-L-C network, where the capacitors are connected as shunt elements to ground and the inductor is connected in series between them. The shunt capacitors provide a low-impedance path for high-frequency components while the series inductor increasingly opposes high-frequency currents. The chosen filter approximation and its microstrip implementation are described in Sections 2.5.1 and 2.5.2.

2.5.1 Chebyshev Approximation

Different filter approximations are used to achieve specific frequency responses. The Butterworth approximation provides a maximally flat response in the passband, while the Chebyshev approximation allows for a sharper transition between the passband and the stopband at the cost of ripple in the passband, as illustrated in Figure 2.1. In this work, the Chebyshev approximation is used due to its improved selectivity, which makes it suitable for evaluating how geometrical modifications affect the filter response. The characteristic ripple behavior of the Chebyshev approximation is visible in the passband region of the filter response shown in Figure 2.1. The power loss ratio for a Chebyshev filter is given by [2]

$$P_{LR}(\omega) = 1 + k^2 T_n^2 \left(\frac{\omega}{\omega_c} \right) \tag{2.4}$$

where k determines the level of passband ripple, ω_c is the cutoff frequency, n is the filter order, and T_n is the Chebyshev polynomial of order n. The Chebyshev polynomials are defined by the recurrence relation

$$T_n(x) = 2xT_{n-1}(x) - T_{n-2}(x) \tag{2.5}$$

with $T_0(x) = 1$ and $T_1(x) = x$. The passband ripple level in dB is given by

$$L_{Ar} = 10\log_{10}(1 + k^2). \tag{2.6}$$

2.5.2 Stepped-Impedance Implementation

At microwave frequencies, ideal lumped inductors and capacitors are replaced by distributed transmission-line sections. A high-impedance transmission-line section approximates a series inductor, while a low-impedance section approximates a shunt capacitor. In a microstrip implementation, these impedance values are realized by changing the conductor width for a given substrate. The equivalent element values for length stepped-impedance sections of electrical θ can be approximated as [2]

$$L \approx \frac{Z_H \sin\theta}{\omega}, \quad C \approx \frac{\sin\theta}{\omega Z_L} \tag{2.7}$$

where Z_H and Z_L are the characteristic impedances of the high- and low-impedance sections, respectively.

Figure 2.4 shows the microstrip implementation used in this work alongside the corresponding lumped-element C-L-C representation. The wider microstrip sections correspond to the capacitive sections with low-impedance (C_1 and C_2), while the narrower central section corresponds to the inductive section with high-impedance (L). The input and output lines are designed for 50 Ω and connect the filter to the ports.

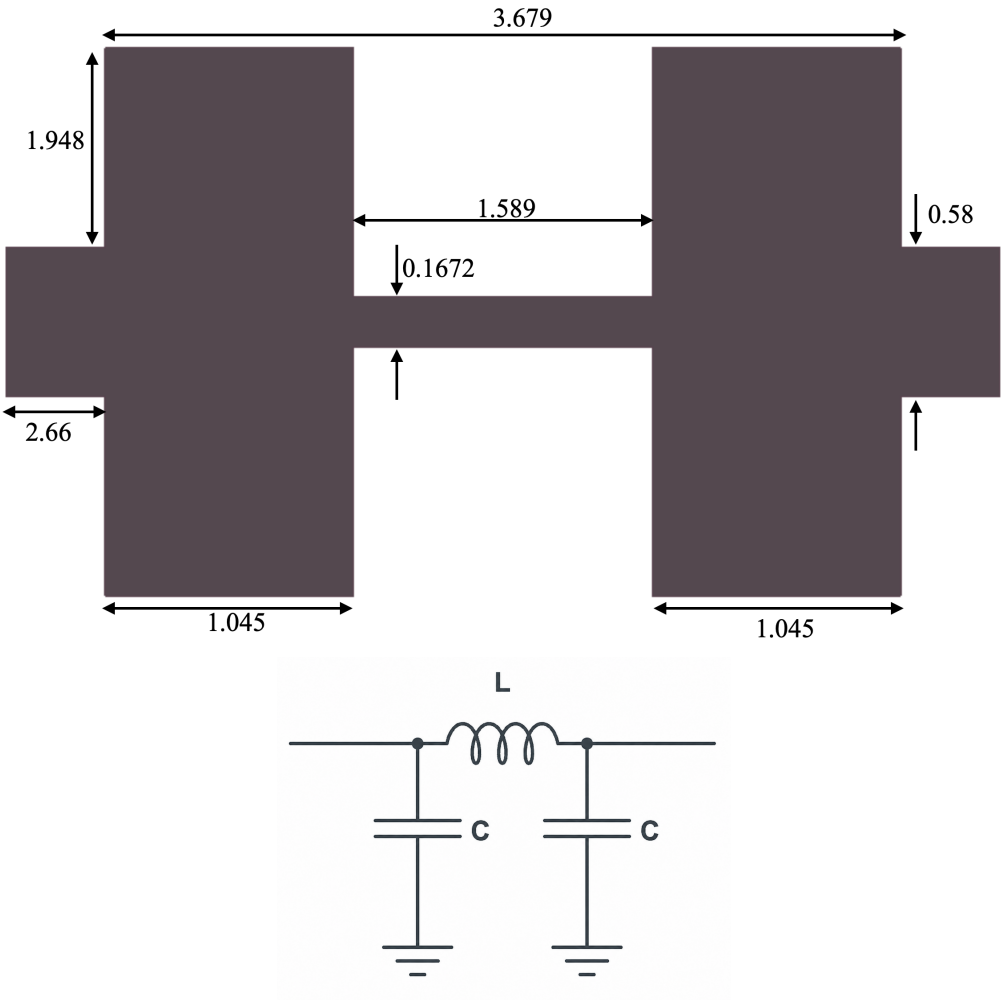

Figure 2.4: Microstrip implementation of the third-order low-pass filter (left) and the corresponding lumped-element C-L-C circuit representation (right). The wider microstrip sections correspond to the capacitive sections C_1 and C_2, the narrower central section corresponds to the inductive section L, and the input and output lines are designed for 50 Ω.

The order of the filter determines the steepness of the transition between the pass-band and stopband. In the third-order filter used in this thesis, the three reactive elements consist of two capacitive sections and one inductive section. This provides a simple and controlled reference structure for investigating how 3D geometrical modifications affect the filter response.

2.6 Three-Dimensional Filter Concepts

The 3D filter concepts extend the conventional planar filter geometries by distributing parts of the conductor, ground plane, or dielectric region in the vertical direction. This provides additional geometrical design freedom compared to planar microstrip implementations, where the signal path and ground reference are arranged in planar horizontal layers.

Additively manufactured electronics provide one possible fabrication route for these types of structures, since conductive and dielectric materials can be deposited in a layer-by-layer process [1]. Previous work has shown that vertically integrated inductive and capacitive structures can be used to miniaturize the microwave filter [3]. These results motivate the investigation of non-planar and multi-level filter geometries in this work.
Moving into three dimensions is not without cost: new electromagnetic effects emerge that can degrade performance if not controlled. Changes in vertical geometry can affect the current distribution, field confinement, coupling between different parts of the structure, and the return current path. Abrupt transitions or modified ground configurations can also introduce impedance mismatches, unintended resonances, or increased losses. 3D filter structures must therefore be evaluated not only in terms of physical size but also in terms of their electromagnetic behavior.

3
Simulation Methodology

This chapter describes the simulation methodology used to investigate the impact of 3D geometries on microwave filter performance. First, the comparative simulation approach is presented and motivated. The common design parameters shared by all investigated models are described. The simulation environment and setup are then explained, and finally the metrics used to evaluate filter performance are introduced.

3.1 Comparative Simulation Approach

The methodology in this thesis is based on a comparative simulation study, with a planar 2D reference filter compared against a series of 3D configurations. The purpose of this approach is to isolate the effect of geometrical modifications on filter performance. The topology, materials, ports, and solver settings are identical in all models. Performance differences between models. Therefore, comes from geometry alone.
None of the models were tuned for the best performance. The point is to see what each 3D approach does to the filter, not to maximize any single design. This supports the aim of the study, which is to understand what each modification does rather than to find the best possible version of any one design.

3.2 Common Design Parameters

All filter configurations in this study are based on the same third-order Chebyshev low-pass filter topology with a target cutoff frequency of 10 GHz, as described in Section 2.5. Model 1, the planar reference filter, serves as the baseline for all comparisons. It represents the conventional 2D microstrip implementation and provides the expected low-pass response against which all 3D configurations are evaluated, as illustrated in Figure 3.1. All 3D models are derived from this reference by modifying selected parts of the geometry while keeping the common design parameters unchanged.
The input and output transmission lines are designed to approximate a characteristic impedance of 50 Ω and are kept identical for all investigated models. This ensures that differences in the simulated responses are not caused by changes in the input and output feed structures.
All simulations use Rogers RO4350B as the dielectric substrate material. This material has a relative permittivity of $\varepsilon_r = 3.66$, and the substrate thickness used in

all simulations is 254 μm, as illustrated in Figure 2.3. Copper was used as the conductor material throughout the study. Fixing material parameters across all models ensures that any performance differences are caused by geometry, not by inconsistent material assumptions.

3.3 Simulation Environment and Setup

All simulations are performed in ANSYS HFSS, a full-wave electromagnetic simulation tool based on the finite element method. The software solves Maxwell's equations numerically in the simulation domain and is widely used for the analysis of high-frequency structures such as filters, antennas, and transmission lines.
The modified models are derived from this setup, but may alter the ground configuration, vertical conductor geometry, or dielectric arrangement in order to investigate 3D filter structures.
Wave ports are used at the input and output of each structure to excite the electromagnetic fields and extract the S-parameters. The same port configuration and characteristic impedance of 50 Ω are used for all simulations, so that differences in the results are not caused by variations in the excitation setup. In the reference model, the dimensions of the wave port are set at 5000 μm height and 10 μm width. The simulation setup for the reference filter, which corresponds to Model 1, is illustrated in Figure 3.1.

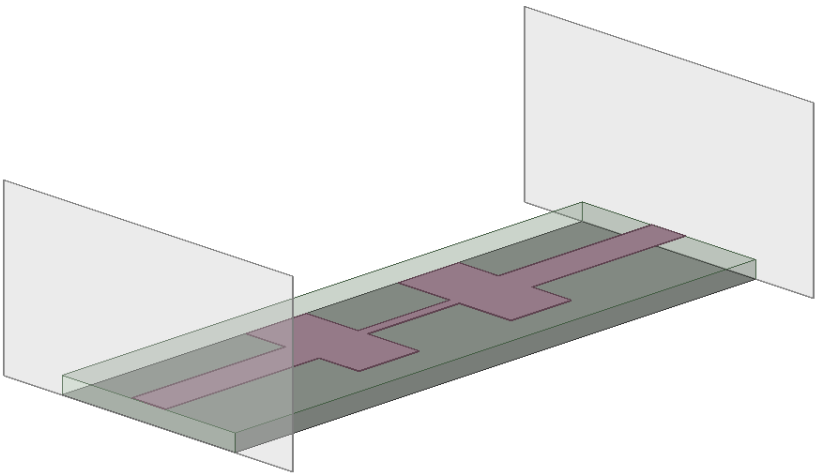

Figure 3.1: HFSS simulation setup for the reference filter, showing the microstrip structure and the wave ports used at the input and output. The two large semi-transparent grey rectangles visible on either side of the structure represent the wave ports.

An open region with a perfectly matched layer boundary (PML) set to a reference frequency of 10 GHz is applied around the simulation domain. The PML boundary is used to absorb outgoing electromagnetic waves and reduce reflections from the domain boundaries, which allows the simulated structure to behave as if it is placed in an open environment. This boundary condition was selected to avoid the artificial

resonances and reflections that would otherwise arise if a closed metallic boundary were used, which would not accurately represent the open-space environment of a microstrip filter.
Adaptive meshing is used to resolve the electromagnetic fields across all designs, with particular attention to regions where strong field variations are expected, such as geometrical discontinuities and transitions between sections of different widths or heights.
The frequency sweep is performed from 5 to 20 GHz for all designs. This range covers both the passband and the stopband of the reference filter and ensures that the cutoff frequency -3 dB can be identified for all investigated configurations.

3.4 Performance Evaluation Metrics

The filter configurations are evaluated using simulated S-parameters exported from HFSS. The main quantities used in the comparison are the transmission coefficient S_{21} and the reflection coefficient S_{11}.
The transmission coefficient S_{21} is used to evaluate insertion loss, cutoff behavior, and stopband attenuation. The cutoff frequency is determined from the response S_{21} using the point -3 dB relative to the maximum value of S_{21}, where a value of approximately -20 dB or below in the stopband is used as an indication of strong attenuation.
The reflection coefficient S_{11} is used to evaluate the impedance matching at the input port, where values below -10 dB are interpreted as acceptable impedance matching in the passband. This threshold corresponds to approximately 10% of the incident power reflecting back toward the source.
For each filter model, the cutoff frequency, the minimum value of S_{11}, and the frequency at which this minimum occurs are extracted from the simulated response to the S-parameter. These values are used to compare how the 3D geometrical modifications affect the filter response relative to Model 1 and are summarized in Table 5.1 in Chapter 5.
Electric field distributions are used as a supporting evaluation method. Field plots at representative frequencies are analyzed in order to identify effects that are not directly visible in the S-parameter response, such as unintended resonances, coupling between different sections, field leakage, and regions of concentrated field energy. Representative frequencies are selected based on the features observed in the response of the S-parameter , such as of the passband operation or the pronounced minima in S_{11}.
Physical size is also considered as a supporting evaluation metric. Both the planar footprint and the total height of each structure are taken into account, since one motivation for 3D filter design is the possibility of reducing the planar area at the cost of increased vertical height. The footprint is evaluated as the projected area of the filter in the horizontal plane, excluding the 50 Ω input and output feed lines, and the total height describes the vertical extent of the structure. The physical dimensions of all models are summarized in Table 4.2 in Chapter 4, and a normalized size comparison is given in Table 6.1 in Chapter 6.

4

Design and Implementation

The filter structures investigated in this study are presented in this chapter. The chapter begins with the design of the 2D reference filter, which serves as the baseline for all comparisons. Thereafter, the 3D filter configurations are presented, organized into three categories: modified ground plane configurations, multi-level conductor structures, and geometrical design variations. For each design, the key geometrical features and the motivation for investigating that particular configuration are described.

Each model targets a specific question; certain models push a design choice to its limit, such as removing the ground plane or compressing the inductive section into a spiral, while others form paired comparisons where two models differ in a single geometrical parameter to isolate its effect. This progression is described in each subsection and summarized in Table 4.1. For each model, the ground plane configuration is illustrated in Appendix A (Figures A.1–A.7), where the ground areas are highlighted to facilitate comparison between the different configurations.

Each investigated filter structure is assigned a model number and a descriptive name. These model names are used throughout the following chapters when presenting and comparing the simulation results.

Table 4.1: Overview of the investigated filter models and their specific purpose in the study.

Model	Name	Main modification	Purpose
Model 1	Reference filter	Planar microstrip baseline	Baseline for all comparisons
Model 2	Ground removed	Ground plane removed beneath the central inductive section	Test the effect of removing the local ground reference beneath the inductive section
Model 3	Vertically separated ground	Two substrates stacked vertically with ground planes connected along the long sides	Test the effect of additional dielectric volume and an additional ground reference
Model 4	Sandwich structure	Filter conductor placed between two substrate layers	Test vertical integration with an embedded conductor
Model 5	Square spiral structure	Inductive section reshaped into a square spiral	Test maximum lateral compression of the inductive section
Model 6	Stepped structure	Inductive section distributed across seven equal vertical steps	Test sensitivity to discrete vertical transitions representative of layer-by-layer printing
Model 7	45-degree structure	Inductive section implemented as a straight conductor at a 45-degree angle	Test smooth vertical transition as idealization of Model 6

The physical dimensions of all investigated models are summarized in Table 4.2. In the table, x denotes the lateral width of the structure, y denotes the length along the main signal propagation direction, and z denotes the total vertical height. All dimensions are given in millimeters and do not include the thickness of the substrate. At this stage, no performance evaluation is performed from these values at this stage. Dimensions are included to support the later comparison of footprint, height, and geometrical trade-offs in Section 6.3 Size and Geometry Trade-Offs.

Table 4.2: Physical dimensions of the investigated filter models. All values are given in mm and do not include substrate thickness.

Model	Name	x	y	z	Additional comments
Model 1	Reference filter	9	3	0.5	Planar baseline.
Model 2	Ground removed	9	3	0.5	Same outer dimensions as Model 1. Ground removed beneath the inductive section.
Model 3	Vertically separated ground	9	3	1	Increased lateral width and height due to stacked substrates.
Model 4	Sandwich structure	2.545	3	1.59	Inner gap between conductor and ground: 1.061 mm.
Model 5	Square spiral structure	2.9022	3	0.528	No ground plane beneath the spiral region.
Model 6	Stepped structure	5.92	3	1.032	Seven equal steps. Vertical extent beneath stepped section: 0.778 mm.
Model 7	45-degree structure	8.53	3	1.37	Smooth angled transition at 45 degrees.

4.1 Reference Filter

Model 1 is the planar reference filter that is used as a baseline for all the comparisons in this thesis. It is implemented as a third-order Chebyshev low-pass microstrip filter on a Rogers RO4350B substrate with a relative permittivity of $\varepsilon_r = 3.66$ and a substrate thickness of 254 μm. The filter is designed for a target cutoff frequency of 10 GHz following the stepped-impedance design approach described in Section 2.5. The filter structure consists of three sections that realize the equivalent lumped-element behavior of the Chebyshev prototype. The two outer sections are wide low-impedance microstrip lines that act as shunt capacitors C_1 and C_2 in the equivalent C-L-C circuit shown in Figure 2.4. The central section is a narrow high-impedance microstrip line that acts as a series inductor L. This relationship between the physical geometry and the equivalent circuit follows directly from the step-impedance approximation described in Section 2.5, where the wider sections realize a lower characteristic impedance and, thereby capacitive behavior, while the narrower sections realize a higher characteristic impedance and thereby inductive behavior [2]. The ground plane is continuous beneath the entire conductor structure; a marked illustration of this configuration is shown in Figure A.1 in Appendix A.

The geometric dimensions of the reference filter sections are given in Table 4.3. The input and output ports are implemented as 50 Ω microstrip lines with a width of 0.58 mm and are connected to wave ports in the simulation environment. A 3D

view of Model 1 implemented in HFSS is shown in Figure 4.1.

Table 4.3: Geometrical dimensions of the reference filter sections. All values are given in mm.

Section	Width	Length
Capacitive sections (C_1 and C_2)	1.948	1.045
Inductive section (L)	0.1672	1.589
Input/output 50 Ω lines	0.580	—

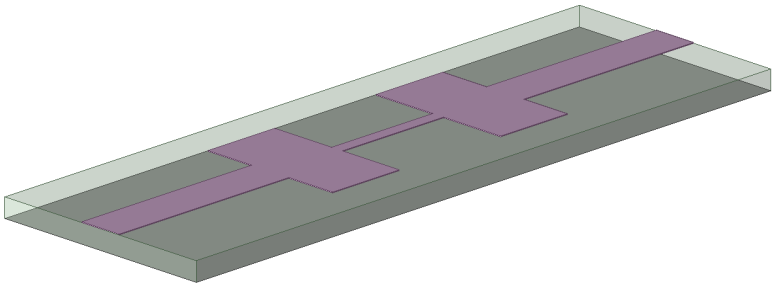

Figure 4.1: Three-dimensional view of Model 1, the reference filter, as implemented in HFSS.

4.2 3D Filter Designs

The 3D filter designs are all derived from the reference filter described in Section 4.1 Reference Filter. Three main categories of modifications are investigated: modifications to the ground plane, multi-level conductor arrangements, and geometrical variations of the signal path. These are described in the following subsections.

4.2.1 Modified Ground Plane Configurations

Two modified ground plane configurations have been investigated. As discussed in Section 2.3 Microstrip Technology, the ground plane provides the return path for the current and confines the electromagnetic fields to the region between the conductor and the ground plane. The two models in this category investigate how different types of ground plane modifications affect this field confinement and the resulting filter behavior.

Model 2 – Ground removed

Model 2 is identical to the reference filter in all respects except that the ground plane beneath the central inductive section has been modified. Rather than a continuous ground plane, the configuration consists of two narrow ground strips running along the outer edges of the substrate, as shown in Figure 4.2. No ground plane is present directly beneath the inductive section, which means that the return current path beneath this section is interrupted. A marked illustration of the ground configuration

is provided in Figure A.2 in Appendix A. Model 2 investigates what happens to the filter behavior when the ground plane continuity beneath the inductive section is broken in this way, while retaining a ground reference along the structural edges.

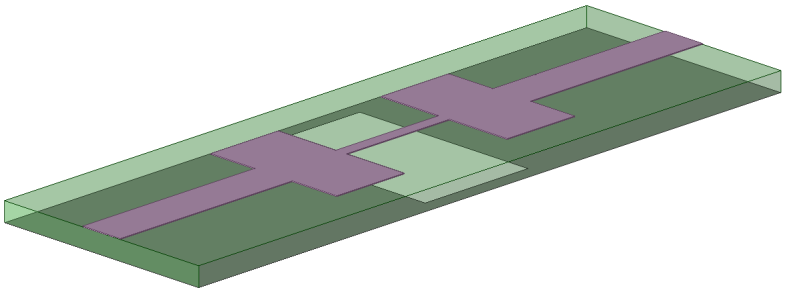

Figure 4.2: Model 2: filter structure with two narrow ground strips running along the outer edges of the substrate. No ground plane is present directly beneath the central inductive section.

Model 3 – Vertically separated ground

Model 3 introduces a vertically separated ground structure, as shown in Figure 4.3. The design consists of two substrates stacked directly on top of each other. The upper substrate carries the filter conductor on its top surface and has a ground plane on its bottom surface, corresponding to the reference filter configuration. The lower substrate adds an additional ground plane to its bottom surface. The two ground planes are connected along the long sides of the structure, forming a 3D ground enclosure around the filter, the full ground configuration is illustrated in Figure A.3 in Appendix A. Model 3 asks whether enclosing the filter in more dielectric and ground material helps or hurts and whether an enclosed ground is a viable strategy for 3D designs.

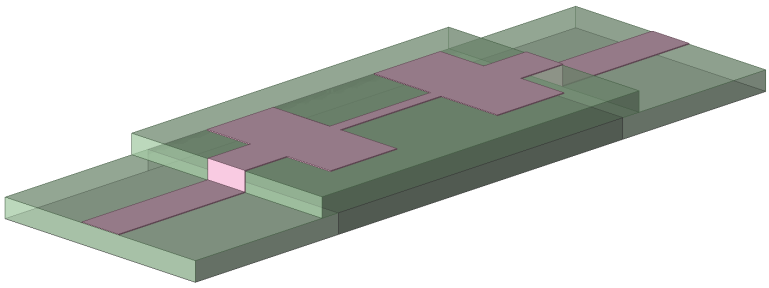

Figure 4.3: Model 3: filter structure with a vertically separated ground configuration consisting of two stacked substrates. The ground planes are connected along the long sides of the structure.

4.2.2 Multi-Level Conductor Structures

Two multi-level conductor configurations have been investigated. These models study how placing the filter conductor at different vertical positions or reshaping it

into a compact 3D geometry influences the electromagnetic behavior and physical size of the filter.

Model 4 – Sandwich structure

Model 4 is a sandwich structure where the filter geometry of the reference filter is folded into a U-shaped shape, as shown in Figure 4.4. From the input wave port, the signal travels horizontally through the 50 Ω input line and the first capacitive section C_1. At the junction between C_1 and the inductive section L, the structure bends 90 degrees downward so that the inductive section runs vertically. At the junction between L and the second capacitive section C_2, the structure bends 90 degrees again, returning to a horizontal orientation so that C_2 runs parallel to and below C_1, before continuing through the 50 Ω feed line and wave port. The conductor is placed on the outer surface of the U-shaped shape, with the substrate following continuously along the entire U-form between the conductor and the ground plane. The ground plane runs along the inner concave surface of the U-shape, as illustrated in Figure A.4 in Appendix A. The total vertical height of the structure is 1.59 mm, with an inner gap of 1.061 mm between the conductor and the ground plane.
The purpose of this model is to investigate how folding the filter geometry into a compact U-shaped shape influences the electromagnetic behavior and whether this type of vertical integration can preserve the low-pass characteristic while enabling a more compact lateral footprint.

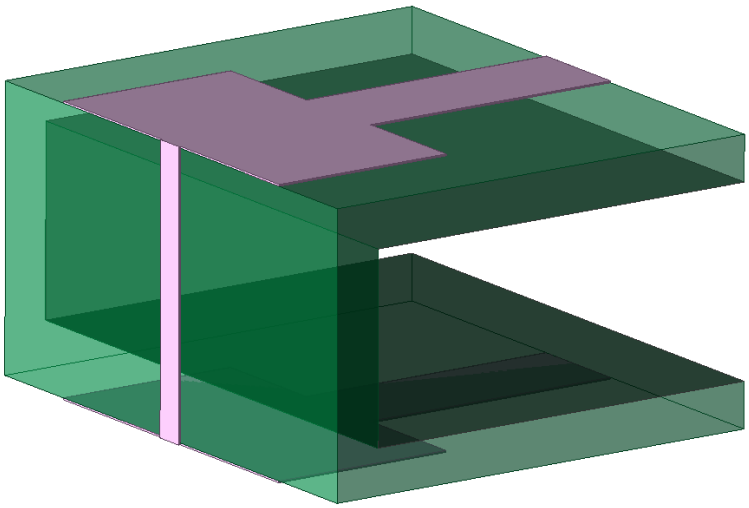

Figure 4.4: Model 4: sandwich structure where the filter geometry is folded into a U-shape. The conductor runs along the outer surface of the U-form, with the substrate continuously following the structure between the conductor and the ground plane, which runs along the inner concave surface.

Model 5 – Square spiral structure

Model 5 is a square spiral structure in which the inductive section of the reference filter is reshaped into a compact square spiral geometry, as shown in Figure 4.5. No

ground plane is placed directly below the spiral region, as can be seen in the marked ground plane view in Figure A.5 in Appendix A. The purpose of this model is to investigate how much the inductive section can be compressed into a smaller lateral area by reshaping it into a spiral and whether an acceptable filter response can be maintained when the inductive section is folded in this way. Model 5 compresses the inductive section as far as possible into a spiral, trading a clean ground reference and straight current path for a much smaller footprint.

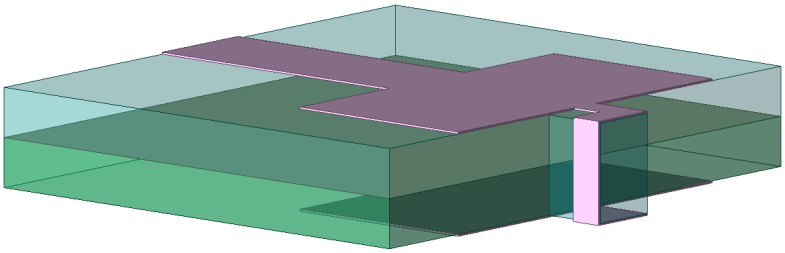

Figure 4.5: Model 5: square spiral structure where the inductive section is reshaped into a compact square spiral. No ground plane is present directly beneath the spiral region.

4.2.3 Geometrical Design Variations

Two geometrical variations of the inductive section have been investigated. These models form a paired comparison, where the inductive section is extended in the vertical direction in two different ways, one with discrete steps and one with a smooth angled transition. The motivation for this pairing is directly related to how additive manufacturing technologies fabricate 3D structures. In inkjet-based AME systems, structures are built layer by layer, which means that any angled or curved surface is inherently approximated by a staircase of discrete steps.

Model 6 – Stepped structure

Model 6 is a stepped structure in which the inductive section is divided into seven equal steps that descend vertically from the upper capacitive section to the lower capacitive section, as shown in Figure 4.6. The width and total length of the inductive section are the same as in the reference filter, with a width of 0.1672 mm and a length of 1.589 mm, but the section is distributed across the vertical dimension through the stepped geometry. The vertical extent below the stepped section is 0.778 mm. The capacitive sections remain planar and are placed at the top and bottom of the stepped inductive section, respectively. A ground plane follows the underside of the stepped structure throughout, as illustrated in Figure A.6 in Appendix A. The purpose of this model is to investigate how sensitive the filter response is to the discrete vertical transitions introduced by the stepped geometry, which is representative of the layer-by-layer nature of additive manufacturing.

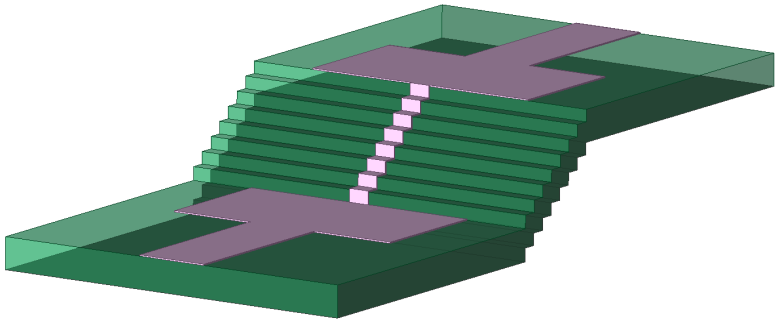

Figure 4.6: Model 6: stepped structure where the inductive section is formed by seven equal vertical steps connecting the two planar capacitive sections. This geometry is representative of how a smooth transition would be approximated by a layer-by-layer additive manufacturing process.

Model 7 – 45-degree structure

Model 7 is a 45-degree structure in which the inductive section is implemented as a single straight conductor at a 45-degree angle connecting the two planar capacitive sections, as shown in Figure 4.7. The width and total length of the inductive section are the same as in the reference filter and Model 6. This model represents the limiting case of the transition used in Model 6, where the discrete steps are replaced by a perfectly smooth angled surface. The ground plane continuously follows the underside of the angled transition continuously, as shown in Figure A.7 in Appendix A. The purpose of this model is to establish whether a smooth vertical transition can preserve the intended filter response and to evaluate how much of the deviation observed in Model 6 is attributable to the abrupt directional changes at each step rather than to the vertical redistribution of the inductive section itself.

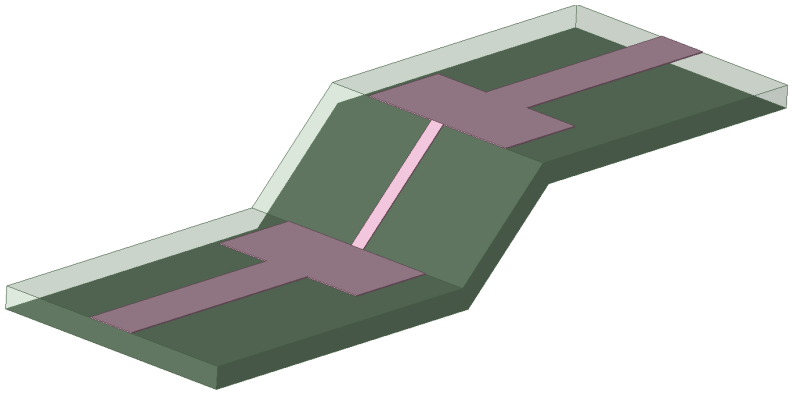

Figure 4.7: Model 7: filter structure where the inductive section is implemented as a straight conductor at a 45-degree angle connecting the two planar capacitive sections. This represents the idealized smooth transition that Model 6 approximates through discrete steps.

5
Simulation Results

This chapter presents the simulated responses to the S-parameter and the electric field distributions for all filter models introduced in Chapter 4. All results are compared with Model 1, the reference filter, which serves as a baseline throughout this chapter. The chapter follows the same structure as Chapter 4, beginning with Model 1 and then presenting the results for the modified ground plane configurations, the multi-level conductor structures, and the geometrical design variations in turn. A summary of the key metrics of the S-parameter for all models is given in Table 5.1. The cutoff frequency -3 dB is defined as the frequency at which S_{21} drops to -3 dB relative to its maximum value. For Model 2, $S_{21,\max}$ is only -5.2 dB relative to the incident signal, which means the filter is strongly degraded throughout the entire frequency range. The reported cutoff frequency of 7.7 GHz for Model 2 is therefore defined relative to $S_{21,\max}$ and should not be interpreted as a meaningful filter cutoff in the conventional sense.

Table 5.1: Summary of key S-parameter metrics for all investigated filter models.

Model	Name	$f_{-3\text{dB}}$ [GHz]	$S_{21,\text{max}}$ [dB]	S_{21} at 20 GHz [dB]	$S_{11,\text{min}}$ [dB]	$f(S_{11,\text{min}})$ [GHz]	$S_{11} < -10$ dB region
Model 1	Reference filter	13.8	−0.15	−9.6	−39.5	8.6	5.00–11.00 GHz
Model 2	Ground removed	7.7*	−5.2	−18.8	−6.5	8.15	None
Model 3	Vertically separated ground	15.05	−0.14	−10.7	−35.7	9.95	5.00–12.46 GHz
Model 4	Sandwich structure	16.85	−0.11	−6.5	−53.6	10.9	5.00–13.70 GHz
Model 5	Square spiral structure	15.2	−0.08	−7.9	−53.3	8.6	5.00–11.79 GHz
Model 6	Stepped structure	16.7	−0.25	−6.4	−22.09	11.6	5.00–13.81 GHz
Model 7	45-degree structure	13.8	−0.17	−9.7	−33.9	8.5	5.00–11.00 GHz

*Defined relative to $S_{21,\text{max}}$, not relative to the incident signal. See Section 5.1 for details.

5.1 Reference Filter Performance

The performance of Model 1 is evaluated using the transmission coefficient S_{21} and the reflection coefficient S_{11}. The cutoff frequency is taken as the frequency at which S_{21} reaches -3 dB relative to its maximum value. The simulated S-parameters are shown in Figure 5.1.

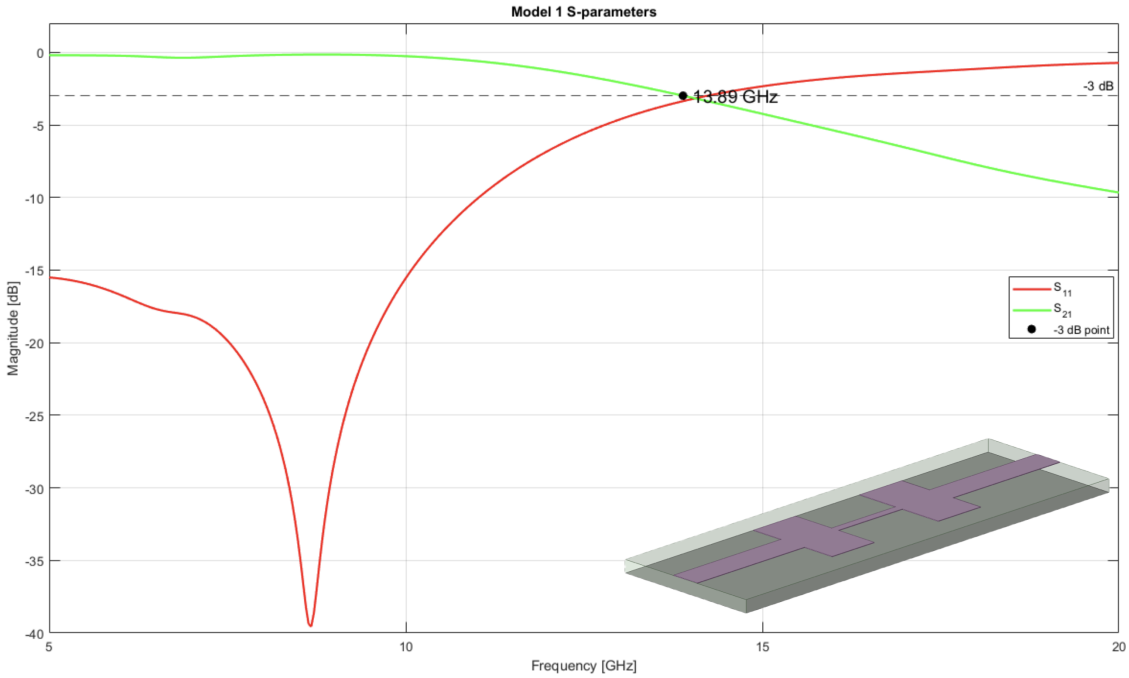

Figure 5.1: Simulated S-parameters (S_{11} and S_{21}) for Model 1, the reference filter. The -3 dB cutoff frequency of S_{21} is approximately 13.9 GHz.

Model 1 performs as expected. The transmission coefficient S_{21} peaks at -0.15 dB and remains flat across the passband, with a clean transition into the stopband. The -3 dB cutoff frequency is approximately 13.9 GHz, which is higher than the design target of 10 GHz. This deviation is expected for a step-impedance implementation, where the approximation of the lumped-element behavior by distributed transmission-line sections introduces frequency-dependent effects that become more pronounced as the electrical length of each section increases [2]. The filter is not optimized, and therefore deviation from the design target is acceptable within the scope of this study, where the primary focus is on comparing the low-pass behavior across different 3D configurations rather than achieving an exact cutoff frequency. The reflection coefficient S_{11} is below -10 dB in the frequency range 5.00–11.00 GHz, indicating an acceptable impedance matching across a large portion of the passband. A pronounced minimum of -39.5 dB is observed at 8.6 GHz, beyond this region, S_{11} increases as the filter approaches the transition and stopband regions, which is consistent with the expected response of a third-order Chebyshev low-pass filter [2]. The distribution of the electric field distribution at a representative frequency within the passband is shown in Figure 5.2.

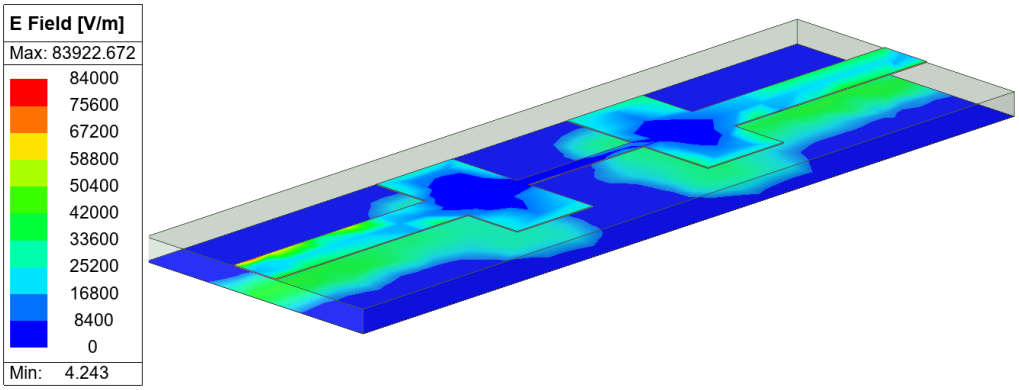

Figure 5.2: Electric field distribution for Model 1 at a representative passband frequency, shown near the conductive sections and the surrounding dielectric region.

The electric field is primarily concentrated near the conductive sections, with a stronger field intensity observed around the wider capacitive sections. This is consistent with the step-impedance design, where larger low-impedance sections realize capacitive behavior through increased electric field coupling to the ground plane [2]. The field is well confined to the vicinity of the transmission line, indicating that the continuous ground plane provides a well-defined return path for the current. Model 1 clearly functions as intended and serves as a solid baseline for the comparisons that follow.

5.2 Modified Ground Plane Configurations

This section compares Model 2 and Model 3 with Model 1 to evaluate the role of the ground plane in maintaining the intended filter behavior. The simulated S-parameters for Model 2 and Model 3 are shown in Figures 5.3 and Figure 5.6, respectively.

Model 2

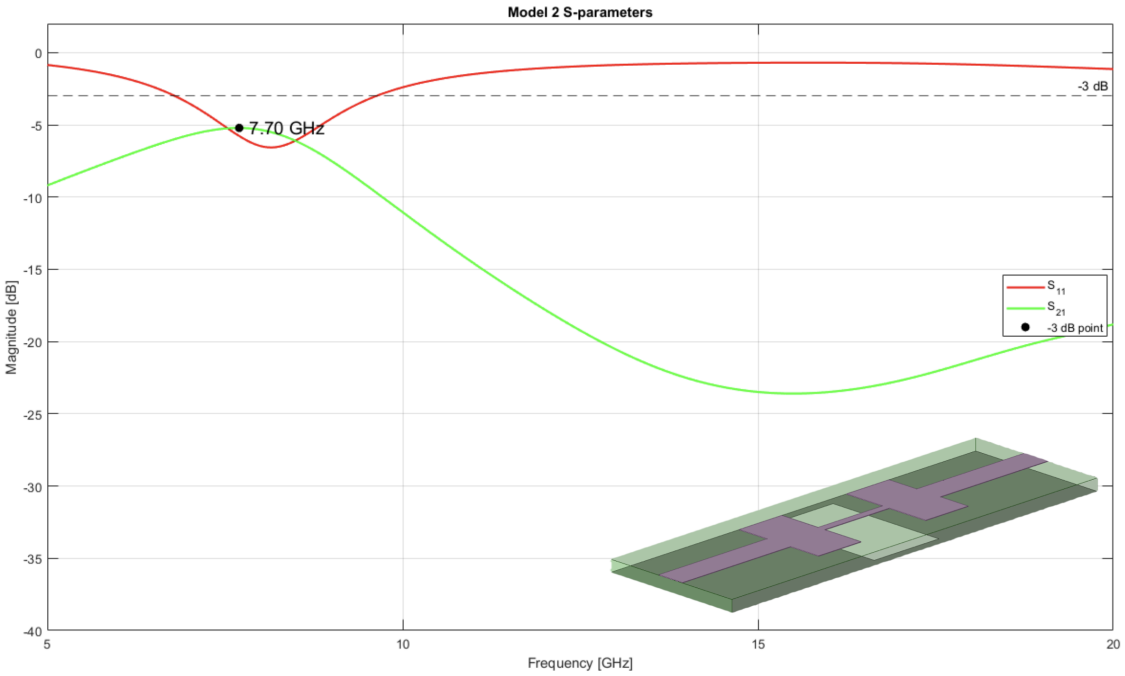

Figure 5.3: Simulated S-parameters for Model 2, where the ground plane beneath the central inductive section has been replaced by two narrow strips along the outer edges of the substrate. Note that the marked point indicates the maximum value of S_{21} at -5.218 dB, not a conventional -3 dB cutoff frequency.

Model 2 shows a significantly degraded response compared to Model 1. The transmission coefficient S_{21} reaches a maximum of only -5.218 dB relative to the incident signal, indicating a substantial loss insertion throughout the frequency range. Since S_{21} never reaches the -3 dB level relative to the incident signal, the conventional cutoff frequency can not be defined for this model. The S_{11} never drops below -10 dB, confirming that the impedance matching is poor throughout. The S-parameter response bears little resemblance to Model 1 and is more consistent with a radiating structure than a filter.

The electric field distribution for Model 2 is shown in Figure 5.4, and a close-up view of the electric field vectors in the transition region between the capacitive and inductive sections is shown in Figure 5.5.

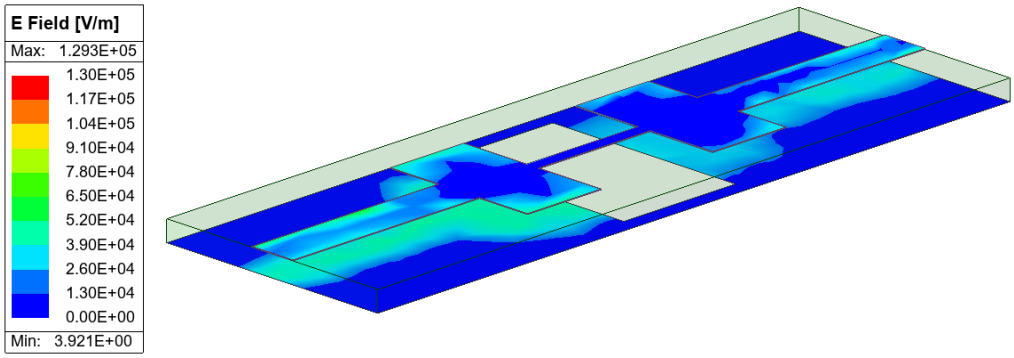

Figure 5.4: Electric field distribution for Model 2, where the ground plane beneath the central inductive section has been replaced by two narrow edge strips.

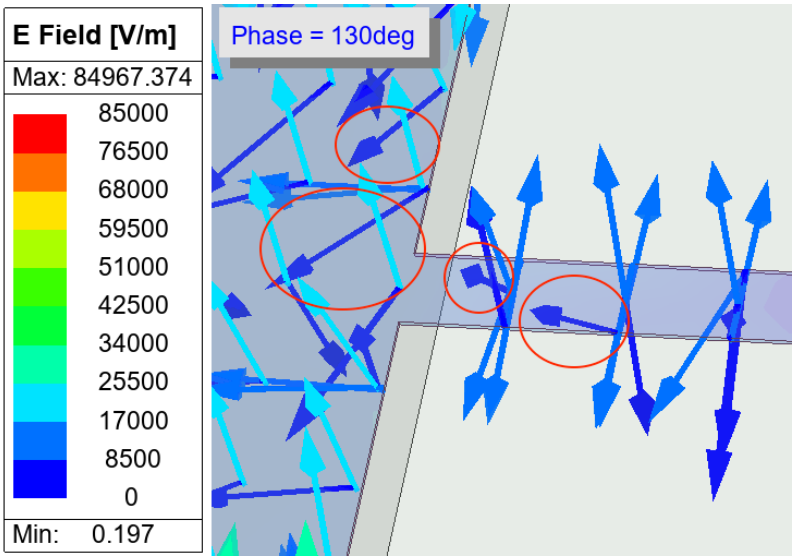

Figure 5.5: Close-up of the electric field vectors in the transition region between the capacitive and inductive sections of Model 2 at 130 degrees phase. The marked vectors show field components directed diagonally toward the edge ground strips rather than being confined directly beneath the inductive section conductor.

In contrast to Model 1 in Figure 5.2, the electric field in Model 2 is no longer confined to the region directly beneath the conductor. The vector plot in Figure 5.5 shows that in the transition region between the capacitive and inductive sections, the field vectors are directed diagonally towards the nearest available ground reference along the structural edges, rather than providing a well-defined return path directly beneath the inductive section. The narrow edge strips are insufficient to maintain the field confinement required for filter operation, and consequently electromagnetic behavior of the structure is dominated by radiation rather than guided wave propagation. This is consistent with the strongly degraded response of the S-parameter observed in Figure 5.3. The physical interpretation of this behavior is discussed further in Chapter 6.

Model 3

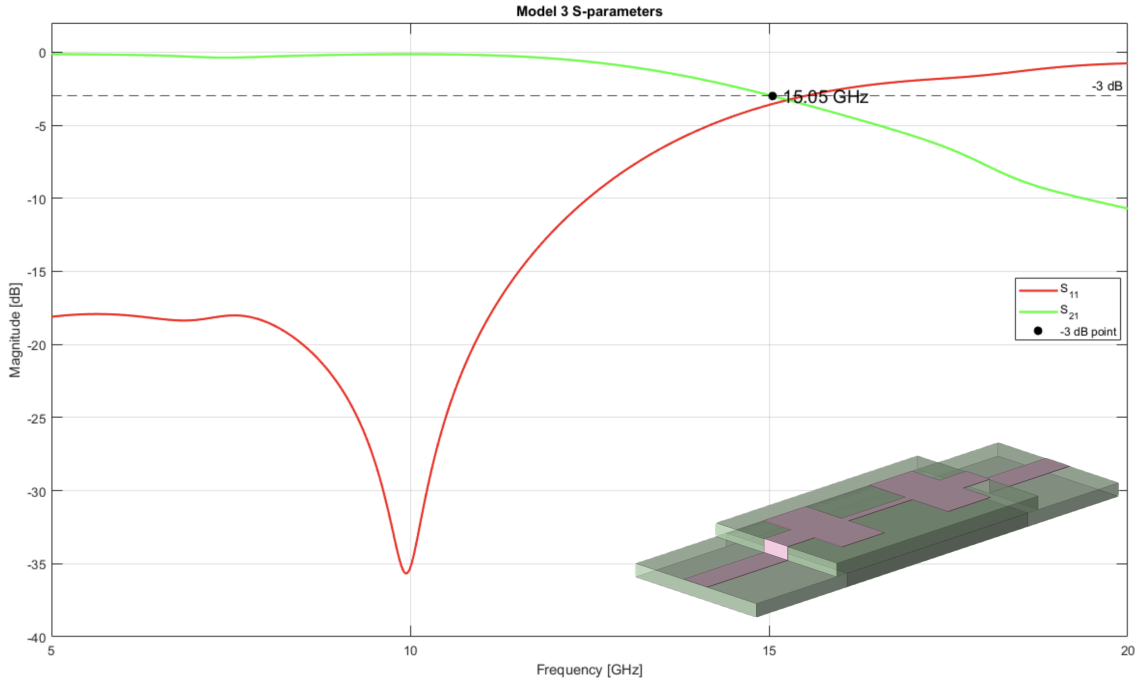

Figure 5.6: Simulated S-parameters for Model 3, the vertically separated ground configuration.

Model 3 shows a different type of deviation from Model 1. The transmission coefficient S_{21} reaches a maximum of -0.14 dB, close to Model 1, with a cutoff -3 dB at 15.05 GHz. The minimum value of S_{11} is -35.7 dB at 9.95 GHz, and S_{11} remains below -10 dB from 5.0 to 12.4 GHz. While the general low-pass characteristic is preserved, a distinct resonance appears in the response to the S-parameter as a sharp local change in both S_{21} and S_{11}.
The S-parameter response of Model 3 is shown in Figure 5.6. A direct visual comparison with Model 1 and all other investigated configurations is provided in Figures 6.1 and 6.2 in Chapter 6.

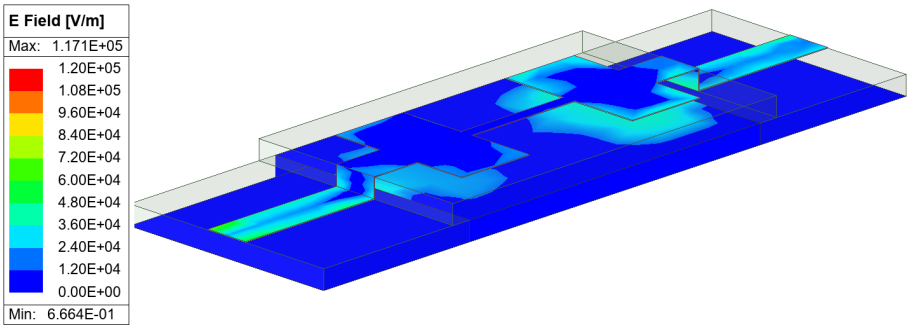

Figure 5.7: Electric field distribution for Model 3, the vertically separated ground configuration.

The electric field distribution for Model 3 is shown in Figure 5.7, showing that the field remains mainly concentrated near the conductive sections and is not strongly spread into the surrounding space. The resonance observed in the S-parameter response is therefore not clearly identifiable from the field distribution alone and is primarily identified from the S-parameter response. The physical interpretation of this behavior is discussed further in Chapter 6.

5.3 Multi-Level Conductor Structures

This section compares Model 4 and Model 5 to evaluate how vertical redistribution of the conductor and ground geometry affects the low-pass filter behavior. The simulated S-parameters for Model 4 and Model 5 are shown in Figures 5.8 and Figure 5.10, respectively.

Model 4

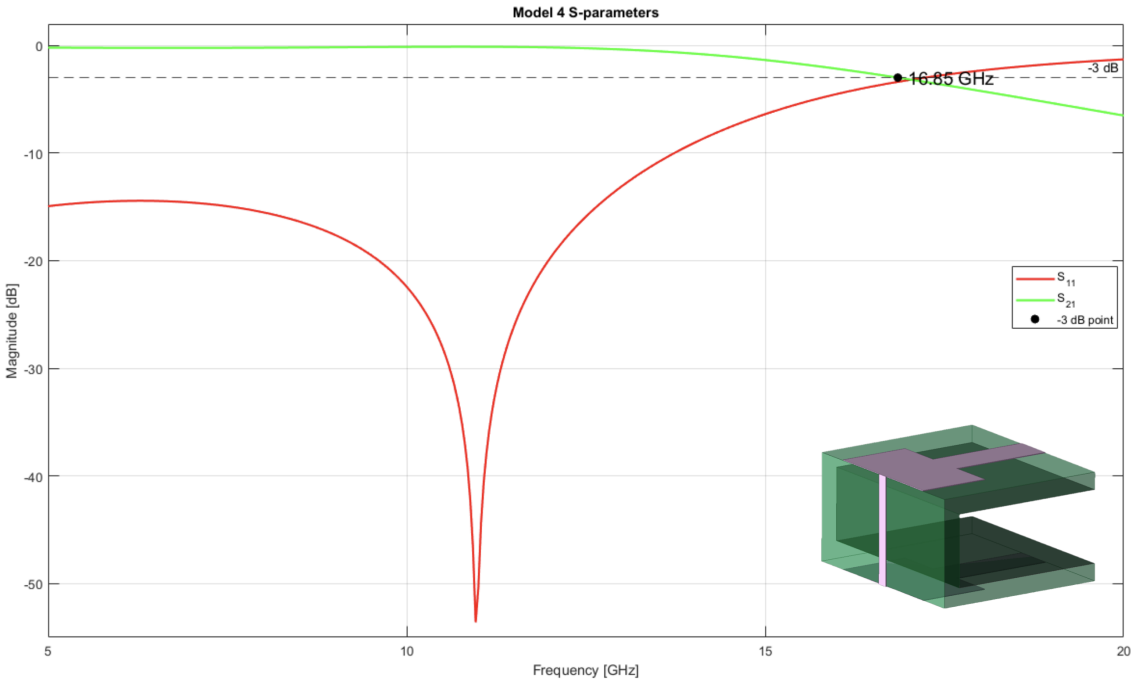

Figure 5.8: Simulated S-parameters for Model 4, the sandwich structure.

Model 4 preserves a clear low-pass characteristic. The transmission coefficient S_{21} reaches a maximum of -0.111 dB with a cutoff point -3 dB cutoff at 16.85 GHz. The minimum value of S_{11} is -53.6 dB at 10.9 GHz, and S_{11} remains below -10 dB from 5.00 to 13.7 GHz. These results indicate that the basic filter topology is still operating despite the significant vertical redistribution of the structure. A pronounced minimum in S_{11} around 10.9 GHz suggests strong local energy storage related to the internal geometry of the sandwich configuration.
The electric field distribution for Model 4 around 10.9 GHz is shown in Figure 5.9.

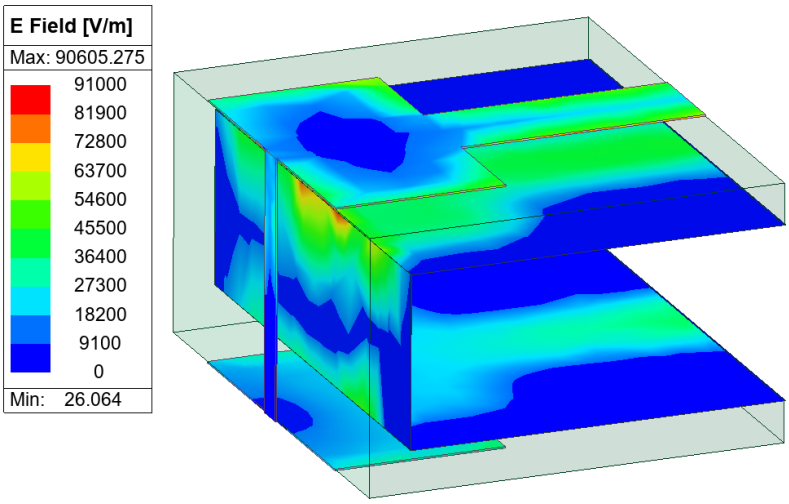

Figure 5.9: Electric field distribution for Model 4 around 10.9 GHz, corresponding to the pronounced minimum in S_{11}.

The electric field distribution for Model 4 shows two distinct behaviors. Near the surface, in the ground plane, the field is not uniformly distributed, with strong concentrations observed near the 90-degree transitions at the vertical connections, indicating localized capacitive coupling at these points. Near the conductive sections, the field is concentrated along the transmission path and becomes particularly intense at the vertical connections, where the current is forced through a geometrically confined path between the different levels of the structure. The field concentrations near the 90-degree transitions suggest that the sharp corners introduce local discontinuities that contribute to the pronounced matching behavior observed in the S-parameter response.

Model 5

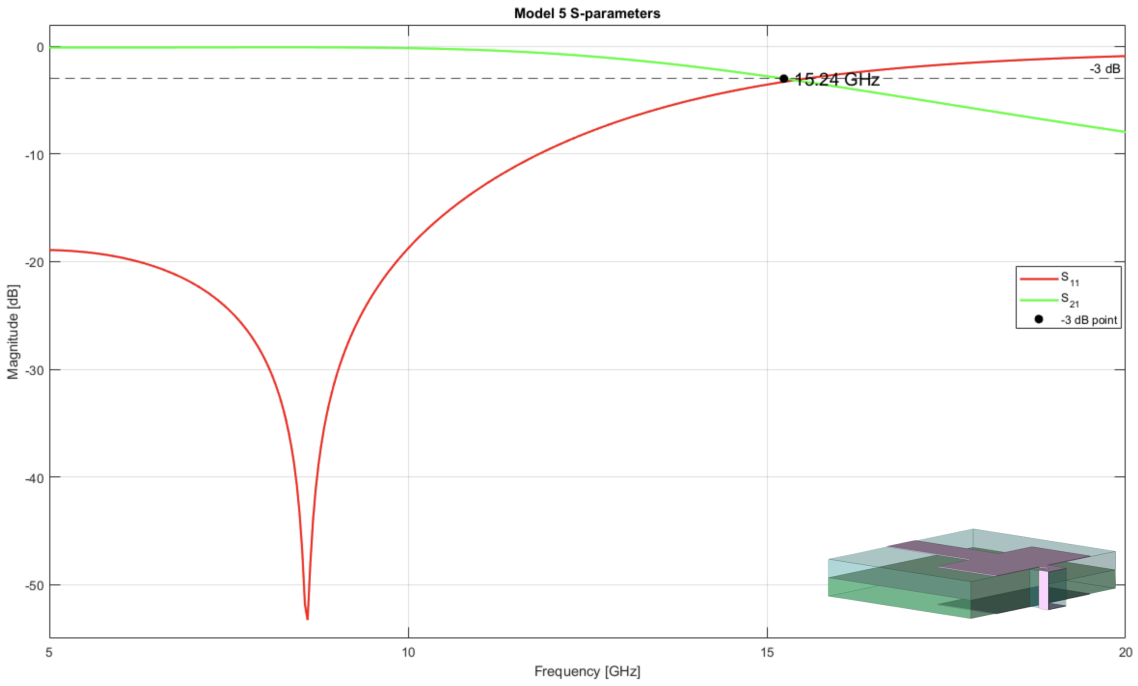

Figure 5.10: Simulated S-parameters for Model 5, the square spiral structure.

Model 5 also preserves the general behavior of the low-pass, but the response differs from Model 1. The transmission coefficient S_{21} reaches a maximum of -0.08 dB with a cutoff point -3 dB at 15.24 GHz. The minimum value of S_{11} is -53.3 dB at 8.6 GHz, and S_{11} remains below -10 dB from 5.00 to 11.8 GHz. None of the investigated models has been optimized for a specific cutoff frequency, and the deviations from Model 1 should be read as indicators of how each geometry shifts the filter response rather than as failures to hit a target.

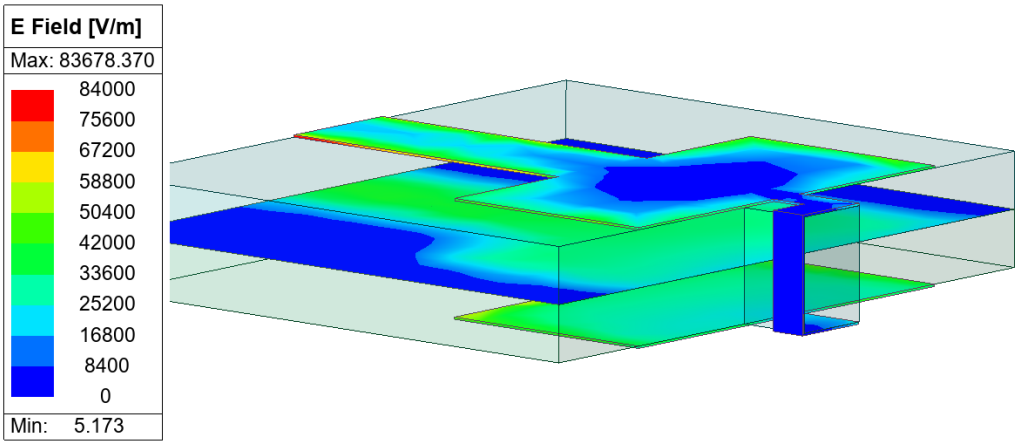

Figure 5.11: Electric field distribution for Model 5 around 8.6 GHz, corresponding to the pronounced minimum in S_{11}.

The electric field distribution for Model 5 around 8.6 GHz is shown in Figure 5.11. Shows that the electromagnetic energy is distributed across larger parts of the structure compared to Model 4. The electric field is present over a wider region near the conductive sections, which is consistent with the modified current path introduced by the square spiral geometry. Since no ground plane is present beneath the spiral region, the field coupling in this region differs fundamentally from the reference design where the ground plane is continuous and provides a well-defined return path. The physical interpretation of these results is discussed further in Chapter 6.

5.4 Geometrical Design Variations

This section compares Model 6 and Model 7 to evaluate how discrete versus smooth vertical transitions in the inductive section affect the filter behavior. As described in Section 4.2.3 Geometrical Design Variations, these two models form a paired comparison where Model 6 uses discrete steps and Model 7 uses a smooth ramped transition. Both models use a ground plane that follows the underside of the structure throughout. The simulated S-parameters for Model 6 and Model 7 are shown in Figure 5.12 and Figure 5.15.

Model 6

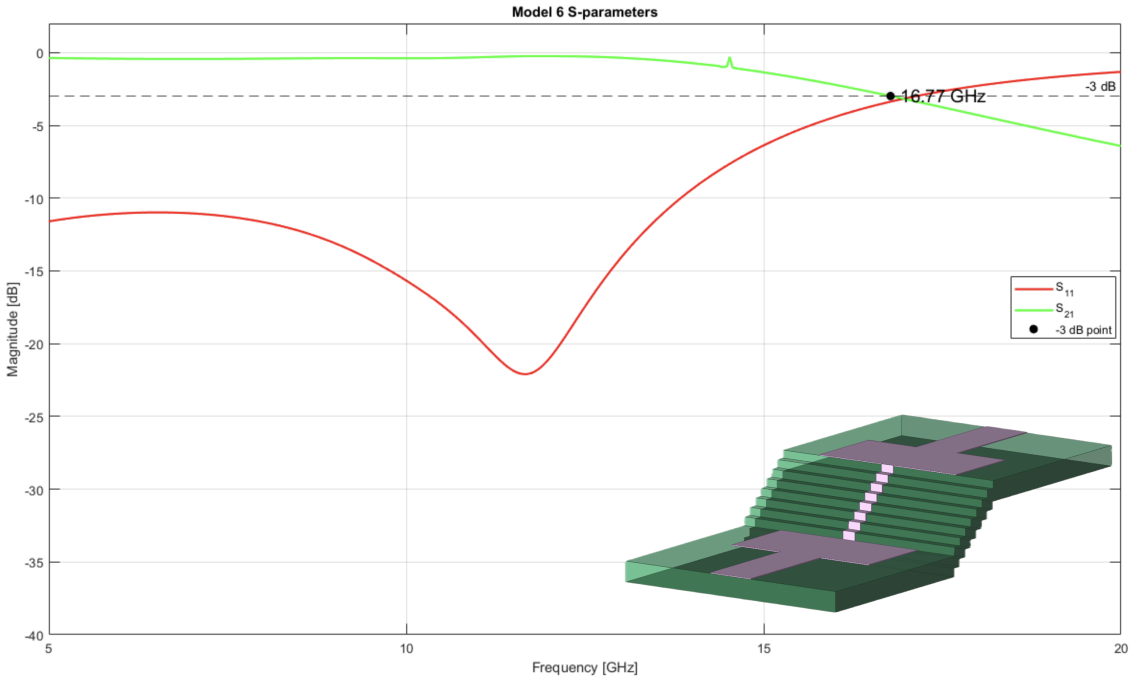

Figure 5.12: Simulated S-parameters for Model 6, the stepped structure.

Model 6 preserves a low-pass characteristic with a cutoff -3 dB at approximately 16.77 GHz. The maximum value of S_{21} is -0.24 dB and S_{21} at 20 GHz is -6.4 dB. The minimum value of S_{11} is -22.09 dB at 11.6 GHz, and S_{11} remains below -10 dB

from 5.0 to 13.8 GHz. Compared to Model 1, the cutoff frequency is shifted upward and the S_{11} minimum is less pronounced, indicating that the stepped geometry affects both the impedance matching and the effective electrical behavior of the inductive section. The electric field distributions for Model 6 are shown in Figure 5.13 and Figure 5.14.

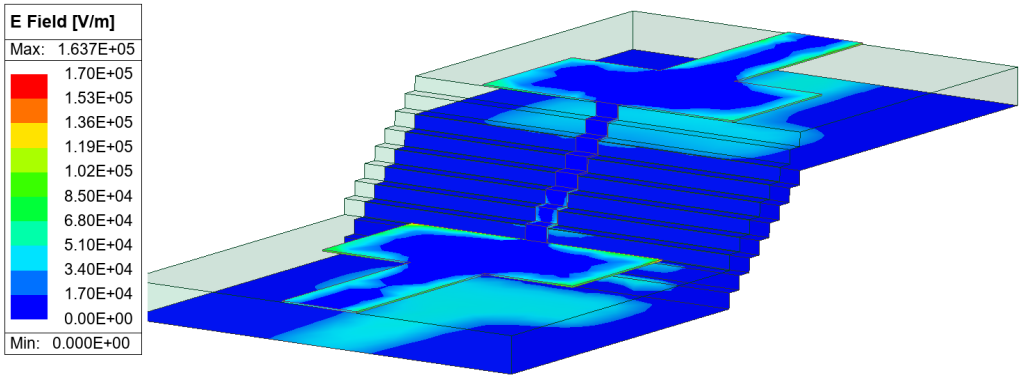

Figure 5.13: Electric field distribution for Model 6, the stepped structure, at a representative frequency.

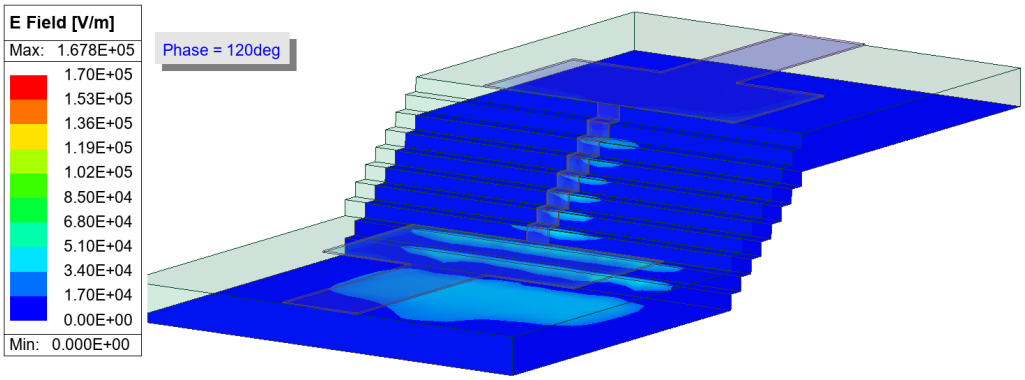

Figure 5.14: Electric field distribution for Model 6 at 120 degrees phase, showing field concentration near the edges of the stepped transitions in the ground plane.

The electric field distribution for Model 6 shows that the field is concentrated near the conductive sections, with increased intensity at the edges of the stepped transitions. The field distribution in the 120 degree phase in Figure 5.14 shows a particularly clear concentration near the edges of the steps in the ground plane, indicating that the sharp corners at each step introduce localized field concentrations. These concentrations give rise to parasitic capacitive and inductive effects that are consistent with the deviation in the filter response compared to Model 1. The detailed analysis of these effects is discussed in Chapter 6.

Model 7

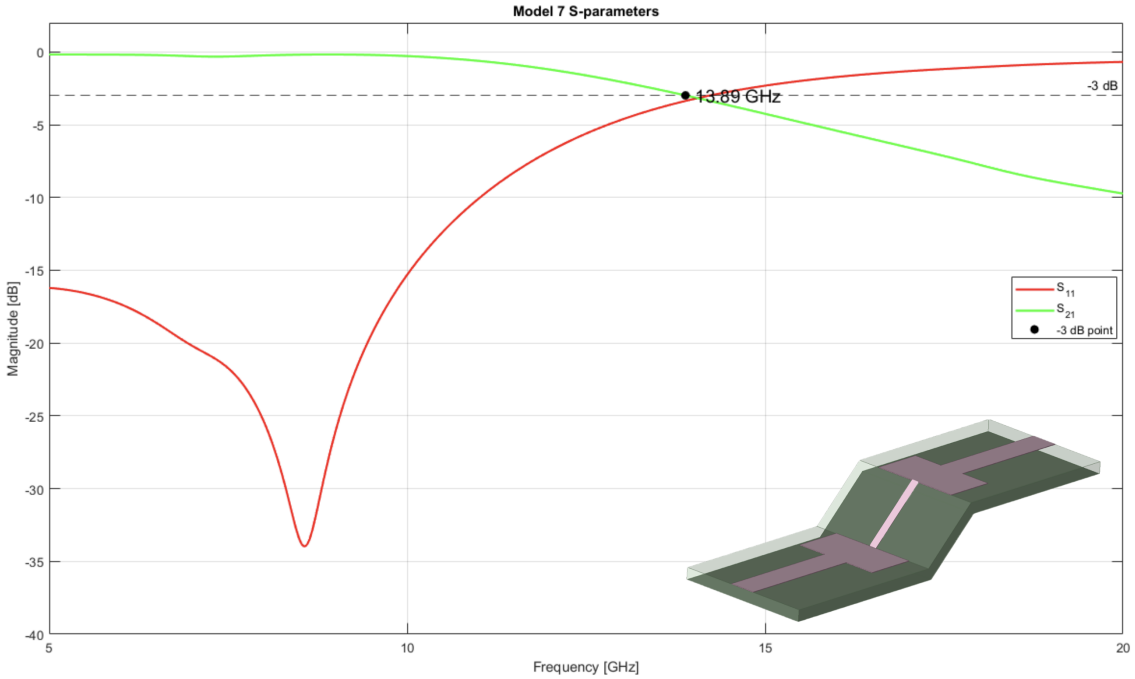

Figure 5.15: Simulated S-parameters for Model 7, the 45-degree structure.

Model 7 shows a response that closely resembles Model 1. The −3 dB cutoff frequency is 13.89 GHz, which is identical to Model 1. The maximum value of S_{21} is −0.17 dB and S_{21} at 20 GHz is −9.7 dB, both close to the corresponding values for Model 1. The minimum value of S_{11} is −33.9 dB at 8.5 GHz, and S_{11} remains below −10 dB from 5.00 to 11.0 GHz, which is identical to Model 1. The electric field distribution for Model 7 is shown in Figure 5.16.

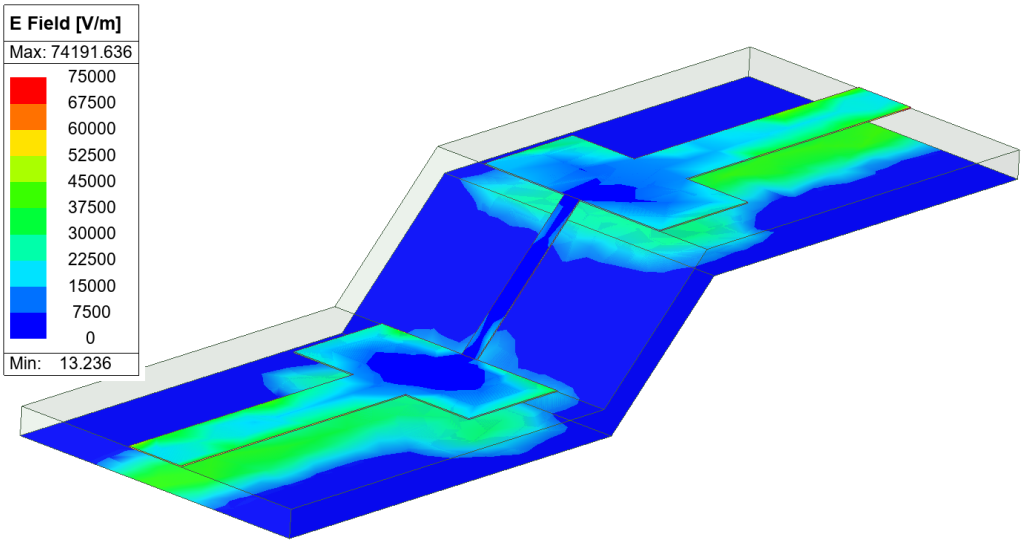

Figure 5.16: Electric field distribution for Model 7, the 45-degree structure, at a representative frequency.

The electric field distribution for Model 7 shows that the field is well confined near the conductive sections and the surrounding dielectric region, with no strong field spreading or pronounced local concentrations at the transition points. This is in contrast to Model 6, where clear field concentrations are observed at the edges of the stepped transitions. The absence of sharp corners in the ramped transition of Model 7 is consistent with the close agreement between its S-parameter response and that of Model 1.

6
Discussion

This chapter discusses the general trends observed in the simulation results and relates them to the research questions stated in Section 1.3. Although Chapter 5 presented the results for each model separately, this chapter focuses on comparing the investigated models as a group in order to identify the main electromagnetic mechanisms, design trade-offs, and implications for 3D microwave filter design enabled by additive manufacturing.

6.1 Overall Performance Trends

The comparison in Figure 6.1 and Figure 6.2 shows that the investigated models exhibit significantly different transmission and reflection behavior. Table 5.1 summarizes the key metrics and is referenced throughout this chapter.

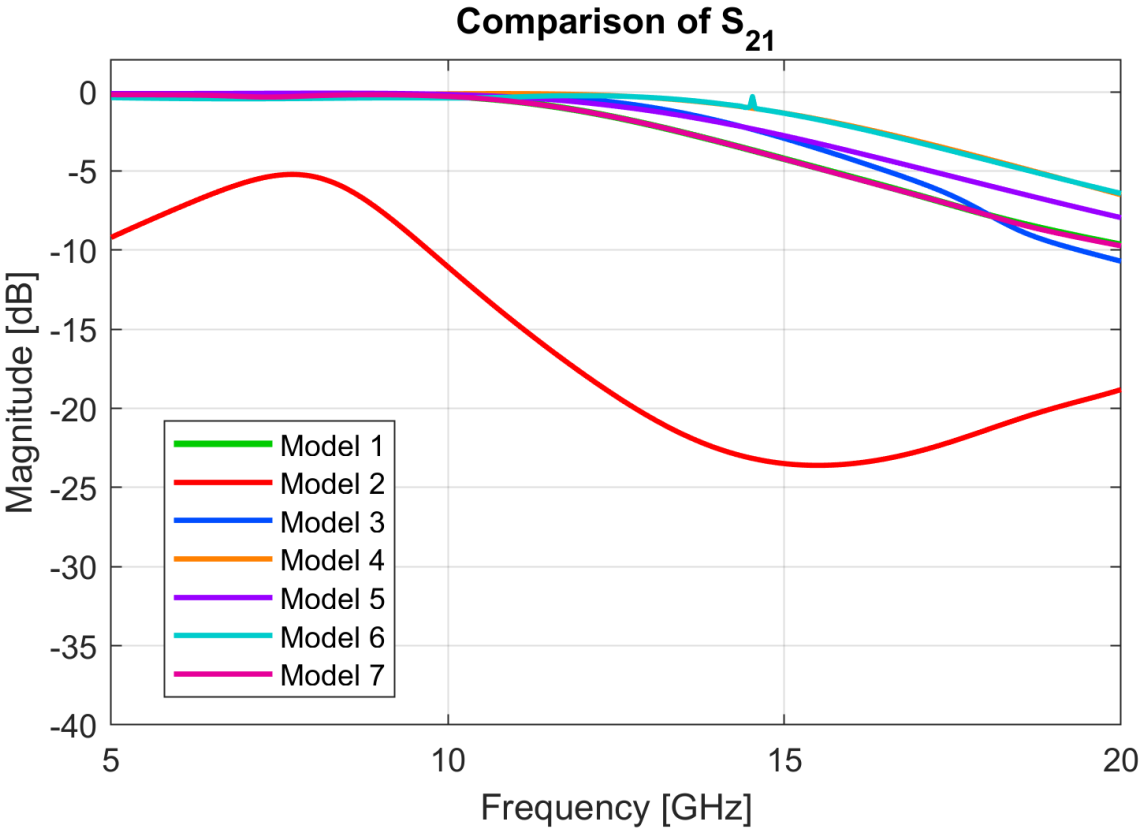

Figure 6.1: Comparison of the simulated transmission coefficient S_{21} for all investigated filter models. Important to note! Model 1 (green) is exactly behind Model 7 (pink) in this figure.

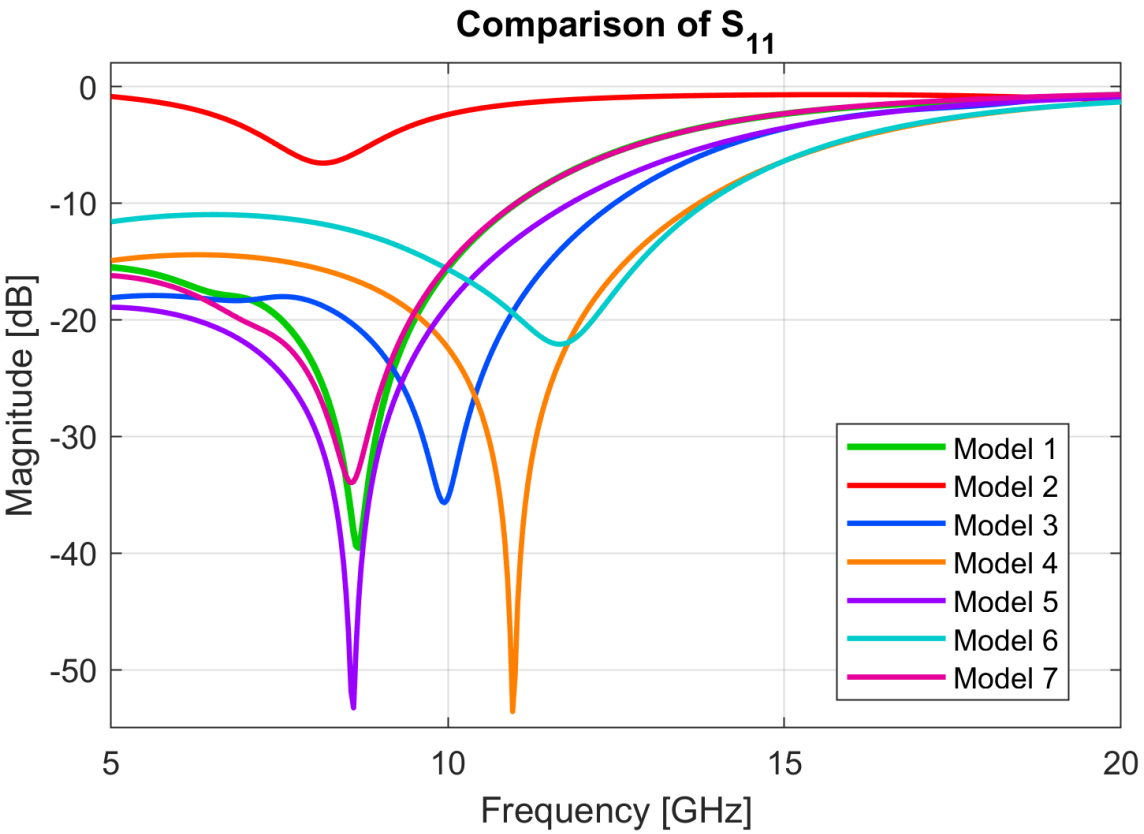

Figure 6.2: Comparison of the simulated reflection coefficient S_{11} for all investigated filter models.

Model 1 (green), the reference filter, provides the baseline response with a -3 dB cutoff frequency of 13.8 GHz and a maximum S_{21} of -0.15 dB. The S_{11} remains below -10 dB from 5.0 to 11.00 GHz with a minimum of -39.5 dB at 8.6 GHz. Although the cutoff frequency is higher than the design target of 10 GHz, the filter shows the expected low-pass transition and is therefore suitable as a baseline for the comparative study.
Model 2 (red), where the ground plane beneath the inductive section is removed, shows the strongest degradation among all investigated models. The maximum S_{21} is only -5.2 dB, indicating substantial insertion loss throughout the entire frequency range, and no meaningful cutoff -3 dB can be defined in the conventional sense since $S_{21,\max}$ itself is only -5.2 dB relative to the incident signal. The S_{11} never drops below -10 dB, confirming poor impedance matching throughout. From a Chebyshev low-pass filter perspective, this model does not function as intended, the characteristic passband, transition band, and stopband regions of the Chebyshev response are not preserved in any meaningful way. The main conclusion from Model 2 is not only that this specific configuration performs poorly but that the inductive section requires a controlled local ground reference to maintain proper filter behavior. Removing the ground plane beneath the inductive section disrupts the return current path and destroys the capacitive coupling that is fundamental to the stepped-impedance filter design.

Model 3 (deep blue), the vertically separated ground configuration, maintains the low-pass characteristic with a cutoff -3 dB at 15.05 GHz and a maximum S_{21} of -0.14 dB. The S_{11} remains below -10 dB from 5.0 to 12.4 GHz with a minimum of -35.7 dB at 9.95 GHz. The main conclusion from Model 3 is that adding more dielectric volume and an additional ground reference is feasible without destroying the filter function.

Model 4 (orange), the sandwich structure, preserves a clear low-pass characteristic with a -3 dB cutoff at 16.85 GHz and a maximum S_{21} of -0.111 dB. The S_{11} minimum is -53.6 dB at 10.9 GHz and S_{11} remains below -10 dB from 5.0 to 13.7 GHz. The basic filter topology therefore still functions despite the significant vertical redistribution of the structure. However, the increased vertical volume and internal ground configuration introduce a pronounced matching minimum that suggests additional resonant behavior related to the internal geometry.

Model 5 (pruple), the square spiral structure, preserves low-pass behavior with a cutoff -3 dB at 15.2 GHz and a maximum S_{21} of -0.08 dB. The S_{11} minimum is -53.3 dB at 8.6 GHz and S_{11} remains below -10 dB from 5.00 to 11.8 GHz. The square spiral geometry changes the effective inductance and capacitance of the structure, which shifts both the cutoff frequency and the impedance matching behavior compared to the reference design.

Model 6 (light blue), the stepped structure, preserves low-pass behavior with a cutoff -3 dB at approximately 16.7 GHz and a maximum S_{21} of -0.25 dB. The S_{11} minimum is -22.09 dB at 11.6 GHz and S_{11} remains below -10 dB from 5.0 to 13.8 GHz. Compared to the other 3D configurations, Model 6 shows the most significant shift in cutoff frequency and the weakest S_{11} minimum, indicating that the stepped geometry introduces more substantial impedance discontinuities than the other designs.

Model 7 (pink), the 45-degree structure, provides the most controlled response among the 3D configurations. The -3 dB cutoff frequency is 13.8 GHz, identical to Model 1. The maximum S_{21} is -0.17 dB and S_{11} remains below -10 dB from 5.0 to 11.0 GHz, identical to Model 1, with a minimum of -33.9 dB at 8.5 GHz. These values are closely comparable to Model 1, indicating that the smooth ramped transition effectively preserves the intended filter behavior when the signal path is extended in the vertical direction.

The maximum transmission coefficient $S_{21,\max}$ provides a direct measure of the insertion loss for each model. Model 2 shows the highest insertion loss with an $S_{21,\max}$ of -5.2 dB, confirming that the disrupted ground reference fundamentally degrades signal transmission. All other 3D configurations show insertion loss values between -0.085 dB and -0.24 dB, which are comparable to the reference filter value of -0.15 dB. These results indicate that with the exception of Model 2, the 3D modifications investigated in this study do not introduce significant additional insertion loss. The differences in filter behavior between these models are therefore primarily related to changes in cutoff frequency, impedance matching, and resonant behavior rather than to increased passband losses.

6.2 Electromagnetic Interpretation

Across all seven models, four effects appear consistently: disrupted return current paths, changed field confinement, shifted effective LC values, and unintended resonances.

6.2.1 Ground Plane Modifications

If this study has one dominant finding, it is that the ground plane matters more than the overall 3D geometry. As established by transmission line theory, a continuous and well-positioned ground plane provides a defined return path for current and confines the electromagnetic fields to the region between the conductor and the ground plane [2]. Model 2 demonstrates the consequences of interrupting this continuity. By replacing the continuous ground plane with two narrow strips along the outer edges of the substrate, the return current path beneath the inductive section is broken. Rather than functioning as a filter, the structure behaves more like a radiating element: the electric field vectors in Figure 5.5 show that the fields in the transition region seek the nearest available ground reference along the structural edges rather than being confined beneath the conductor. The narrow edge strips are insufficient to re-establish the field confinement required for stepped-impedance filter operation.

The key conclusion from Model 2 is therefore not about filter performance, but about ground plane continuity in 3D structures. Even a partial interruption of the ground plane, in this case, retaining edge strips while removing the central ground region, is sufficient to fundamentally alter the electromagnetic character of the device. In a 3D filter design context, this means that any modification that breaks the continuity of the ground plane beneath a filter section must be approached with great care, as the resulting structure may radiate rather than filter. Model 3 shows that adding more ground reference and dielectric volume can preserve low-pass behavior, but the enclosed geometry between the two ground planes introduces cavity-like resonant modes. Although the electric field distribution of Model 3 is visually similar to that of the reference filter, the S-parameter response reveals resonant effects that are not apparent from the field plots alone. This indicates that the S-parameters and field distributions should be interpreted together rather than as standalone evaluations. The behavior of structures where the ground plane is absent beneath parts of the filter, as in Model 5, is discussed further in Section 6.2.2.

6.2.2 Multi-Level Conductor Structures

Model 4 demonstrates that embedding the conductor within a 3D ground enclosure can preserve the low-pass characteristic, but the increased vertical electrical volume allows stronger vertical field interaction than in the planar reference. The pronounced matching minimum around 10.9 GHz, together with the field concentrations observed at the 90-degree transitions in the ground plane, suggests that localized resonant behavior is introduced by the internal geometry.

Model 5 shows that reshaping the inductive section into a square spiral changes

the effective LC balance of the structure. The absence of a local ground reference directly beneath the spiral region modifies the field coupling in this region, and the strong field concentrations observed at the 90-degree corners of the spiral indicate that the current is forced to change direction abruptly at each corner. These effects contribute to the shifted impedance matching behavior compared to the reference design. Despite the absence of a ground plane directly beneath the spiral, the structure retains an acceptable low-pass filter behavior. This can be attributed to the fact that the ground planes beneath the adjacent capacitive sections remain close to the spiral region, providing a sufficiently controlled return current path, as illustrated in Figure A.5 in Appendix A. This is in contrast to Model 2, where the broken ground continuity leaves the return current path insufficiently defined, causing the structure to behave as a radiating element rather than a filter.

6.2.3 Geometrical Design Variations

Model 6 demonstrates the sensitivity of the filter response to discrete geometrical transitions. The sharp corners at each step introduce abrupt impedance discontinuities that give rise to parasitic capacitances and inductances, modifying the values of the effective component values and shifting the cutoff frequency to approximately 16.7 GHz. The electric field distribution at 120 degree phase shows a particularly clear concentration of field energy at the edges of the stepped transitions in the ground plane, confirming that the corners are a primary source of electromagnetic disturbance in this design. Model 7 demonstrates the opposite tendency. By replacing the discrete steps with a smooth 45-degree transition, the abrupt impedance discontinuities are eliminated, and the filter response closely resembles that of the reference design. The comparison between Model 6 and Model 7 directly shows that the shape of the vertical transition is a critical design parameter and that smooth transitions are strongly preferable to abrupt stepped transitions when extending the signal path in the vertical direction.

6.3 Size and Geometry Trade-Offs

One of the motivations for the design of the 3D microwave filter is the possibility of reducing or redistributing the planar footprint of the filter. The footprint and height of all investigated models are summarized in Table 6.1.

Table 6.1: Footprint, height, and normalized size for all investigated filter models. Footprint is defined as $x \times y$, excluding the 50 Ω input and output feed lines. Normalized values are given relative to Model 1.

Model	Footprint [mm^2]	Height z [mm]	Norm. footprint	Norm. height
Model 1	27.00	0.50	1.00	1.00
Model 2	27.00	0.50	1.00	1.00
Model 3	27.00	1.00	1.00	2.00
Model 4	7.64	1.59	0.28	3.18
Model 5	8.71	0.53	0.32	1.06
Model 6	17.76	1.03	0.66	2.06
Model 7	25.59	1.37	0.95	2.74

Table 6.1 highlights some key trade-offs. Model 2 has the same footprint and height as the reference filter since only the ground plane is modified, not the outer geometry. Model 3 has the same footprint as the reference filter but increases the height by a factor of 2 compared to Model 1, making it the least compact structure in the vertical direction among the investigated models while maintaining the same planar area.

Model 4 achieves the largest footprint reduction among all investigated models with a normalized footprint of 0.28 relative to Model 1, at the cost of a height increase by a factor of 3.18. Model 5 achieves a similar footprint reduction with a normalized footprint of 0.32 while maintaining a height close to the reference filter at a normalized height of 1.06, making it the most compact design in terms of total volume. Model 6 achieves a moderate footprint reduction to 0.66 of the reference, while Model 7 has a footprint of 0.95, very close to Model 1.

Size is not the only thing AME changes. It also opens up integration possibilities that conventional PCB manufacturing cannot offer. Model 7 has potential for vertical integration with other planar components. Since the 45-degree structure occupies a controlled vertical space above the capacitive sections, it could in principle be placed over another flat filter or circuit component, allowing two filters to share the same planar area. This integration potential has not been verified in this study and would require further investigation, but it represents a design possibility enabled by the geometrical freedom of additive manufacturing that is not achievable with conventional planar PCB technology. Similarly, the sandwich structure of Model 4 creates an enclosed interior space that could potentially be used to embed other passive components, further increasing the integration density.

A complete SWaP-C evaluation, including weight, power handling, and manufacturing cost, is beyond the scope of this thesis. The size comparison presented here focuses on footprint and height as primary geometrical metrics.

6.4 Qualitative Assessment

Based on the results presented in Chapter 5 and the discussion above, a qualitative assessment of each model is given in Table 6.2. The assessment considers three dimensions: how well the low-pass behavior is preserved compared to Model 1, whether the model offers a size advantage, and whether the model has potential for integration with other components. These ratings reflect what each design achieves without optimization, not what it could achieve with further tuning. Models that show limited performance in the current configuration may still have potential if further optimized.

Table 6.2: Qualitative assessment of all investigated filter models. Ratings: **Good** = close to reference or clearly advantageous, **Limited** = preserved but with deviations, **Poor** = strongly degraded or disadvantageous.

Model	Low-pass behavior	Size advantage	Integration potential
Model 1	Good (baseline)	None (baseline)	Limited
Model 2	Poor	None	None
Model 3	Limited	Poor	Limited
Model 4	Limited	Good	Good
Model 5	Limited	Good	Limited
Model 6	Limited	Limited	Limited
Model 7	Good	Limited	Good

Model 7 is the most promising 3D configuration in terms of preserving the intended filter behavior, while Models 4 and 5 offer the greatest size advantages at the cost of modified frequency responses. Model 2 is the only configuration that shows no potential for further development in its current form, as the removal of the ground plane beneath the inductive section fundamentally disrupts the filter function. All other models preserve the low-pass characteristic to some degree and could potentially be improved through geometrical optimization.

The results also highlight a key advantage of additive manufacturing for microwave filter design: the ability to realize 3D geometries that are not achievable with conventional planar PCB technology. Conventional PCB manufacturing constrains the conductor geometry to predefined planar layers and drilled vias, which limits the design freedom for 3D signal routing and ground configurations. In contrast, additive manufacturing based on AME enables the simultaneous deposition of conductive and dielectric materials in arbitrary 3D geometries [1], making it possible to realize structures such as Model 7, 45-degree transition, Model 4, sandwich configuration, and Model 5, the spiral geometry investigated in this study. Even in cases where the current configurations do not achieve performance identical to the reference filter, the design freedom enabled by additive manufacturing provides a foundation for further optimization that is not available with conventional manufacturing approaches.

6.5 Manufacturing Sensitivity

The sensitivity of each filter configuration to geometrical tolerances is an important consideration when evaluating the practical feasibility of 3D filter designs fabricated using additive manufacturing. Although a systematic tolerance study is outside the scope of this work, the results provide a basis for a qualitative assessment of how sensitive each model is to deviations from the intended geometry.
Model 1 and Model 2 are the least sensitive to geometrical tolerances among the investigated configurations, since their geometries are entirely planar and consist of simple rectangular sections. Small deviations in conductor width or length would slightly shift the cutoff frequency but would not fundamentally alter the filter behavior.
Model 3 introduces a vertically stacked substrate configuration where the separation between the two ground planes determines the resonant behavior of the structure. Since the resonance frequency is directly related to the vertical separation, this model is expected to be moderately sensitive to tolerances in substrate thickness and layer alignment.
Model 4 and Model 5 both involve more complex 3D geometries where the electromagnetic behavior depends on the precise positioning of the conductor relative to the surrounding ground structure. For Model 4, deviations in the inner gap between the conductor and the ground planes would directly affect the impedance and resonant behavior. For Model 5, tolerances in the spiral geometry, including conductor width, spacing, and the position of the spiral relative to the capacitive sections, are expected to influence the cutoff frequency and impedance matching.
Model 6 and Model 7 are expected to be the most sensitive to geometrical tolerances among the investigated configurations. For Model 6, the sharpness and uniformity of each step in the inductive section directly determine the parasitic capacitances and inductances introduced at each transition. Small deviations in step height or step width could therefore shift the frequency response in an unpredictable way. For Model 7, the angle and smoothness of the 45-degree transition are critical parameters. Since the close agreement between Model 7 and Model 1 depends on the absence of abrupt directional changes, any deviation from a perfectly smooth transition, for example due to the layer-by-layer discretization of the printing process, could introduce effects similar to those observed in Model 6. This observation is particularly relevant for additive manufacturing, where the effective smoothness of the transition depends directly on the layer thickness of the printing process.

6.6 Relation to the Research Questions

The main research question in this thesis concerns whether 3D microwave filter structures can improve performance or reduce physical size compared to conventional 2D designs. The results show that 3D structures can preserve the low-pass filter function in several cases but do not automatically improve electromagnetic performance. Model 7 demonstrates that a carefully controlled 3D transition can preserve the filter response to a degree that is closely comparable to the reference

design, with a −3 dB cutoff frequency of 13.8 GHz, identical to Model 1. Models 4 and 5 demonstrate that significant footprint reductions are achievable, down to 28% and 32% of the reference footprint, respectively, but at the cost of modified frequency responses and increased height, as shown in Table 6.1.

The first sub-question concerns how selected 3D geometrical modifications affect insertion loss, return loss, cutoff frequency, and physical size. The results, summarized in Table 5.1 and Table 6.1, show that these parameters are strongly affected by ground configuration, transition shape, and vertical coupling. Removing the ground plane beneath the inductive section causes severe degradation in both the transmission and reflection behavior. Other configurations preserve the low-pass response but shift the cutoff frequency or introduce strong matching minima, indicating that the effective inductance and capacitance of the filter are changed by the 3D geometry. In terms of physical size, Models 4 and 5 achieve the largest footprint reductions, while Model 3 significantly increases both footprint and height significantly.

The second sub-question concerns how the geometrical modifications affect the electromagnetic field distribution and impedance behavior of the filter. The results show that well-controlled structures confine the fields near the intended transmission path, while disrupted ground references or abrupt discontinuities cause field spreading, local concentrations, and resonant behavior. The field analysis of Model 6 in particular shows that field concentrations at the edges of the stepped transitions in the ground plane are directly related to the observed shift in frequency response, confirming that the S-parameter deviations are closely linked to local electromagnetic effects at the geometrical discontinuities.

The third sub-question concerns the trade-offs between filter performance, miniaturization, and geometrical complexity. The results show that increasing the use of the third dimension can reduce the planar footprint, but this is generally accompanied by additional electromagnetic effects that must be controlled. The designs that performed best share three characteristics: a continuous return path, smooth transitions, and well-confined fields. The 45-degree structure demonstrates that these conditions can be satisfied in a 3D implementation and represents the most promising direction for further development among the configurations investigated in this study.

7
Conclusion

7.1 Conclusions

This study has investigated whether three-dimensional microwave filter structures, enabled by additive manufacturing, can improve performance or reduce the physical size of microwave filters compared to conventional two-dimensional designs. The investigation was conducted through full-wave electromagnetic simulations in HFSS, where Model 1, a two-dimensional reference filter, was compared with six three-dimensional configurations. The key metrics of the S-parameter for all models are summarized in Table 5.1 and the physical dimensions are given in Table 4.2 and Table 6.1.

The results show that three-dimensional modifications can preserve acceptable microwave filter performance, but only when the electromagnetic behavior of the structure remains well controlled. Among the three-dimensional configurations investigated, Model 7, the 45-degree structure, showed the most controlled response. The -3 dB cutoff frequency of Model 7 is 13.8 GHz, compared to 13.8 GHz for Model 1, and the responses S_{21} and S_{11} are closely comparable to the reference filter in the investigated frequency range. A direct comparison of the S-parameter responses for Model 1 and Model 7 is shown in Figure 7.1.

In terms of physical size, Models 4 and 5 achieved the largest reductions in planar footprint, with normalized footprints of 0.28 and 0.32 relative to Model 1, respectively, as shown in Table 6.1. However, these reductions came at the cost of modified frequency responses and, in the case of Model 4, a height increase by a factor of 3.18. Model 7 achieved a footprint of 0.95 relative to Model 1 with a height increase by a factor of 2.74. These results show that size reduction is achievable through three-dimensional design, but is generally accompanied by changes in electromagnetic behavior that must be carefully managed.

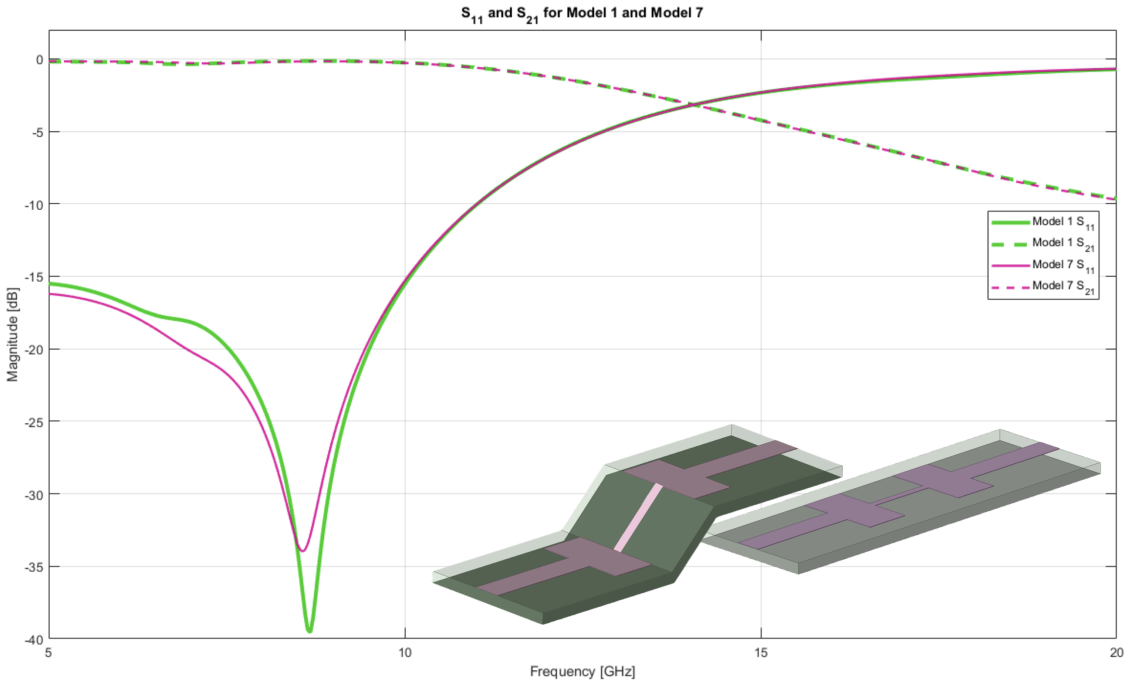

Figure 7.1: Comparison of the simulated transmission coefficient S_{21} for Model 1 and Model 7 and comparison of the simulated reflection coefficient S_{11} for Model 1 and Model 7.

The results further show that the ground plane configuration is critical for maintaining field confinement and acceptable impedance matching. Removing the ground plane beneath the inductive section in Model 2 disrupted the return current path and caused the electromagnetic fields to spread into the surrounding space, which strongly degraded the S-parameter response. As shown by the electric field vectors in Figure 5.5, the field in the transition region was redirected diagonally toward the nearest available ground reference rather than being confined directly beneath the inductive section. The vertically separated ground configuration in Model 3 introduced additional resonant behavior, showing that modifying the ground structure can create unintended electromagnetic effects even when the electric field distribution appears visually similar to the reference filter. These results confirm that a controlled and continuous ground reference is essential when extending microwave filter structures to three dimensions.
The comparison between Model 6 and Model 7 shows that the shape of the transition between filter sections has a significant influence on the filter response. Model 6 preserved the low-pass characteristic but introduced abrupt impedance discontinuities at each step, as confirmed by the electric field concentrations observed at the step edges in the ground plane, and the cutoff frequency shifted to approximately 17.0 GHz. Model 7 used a smoother 45-degree transition and maintained the intended response more effectively, with a cutoff frequency of 14.038 GHz closely matching Model 1. This paired comparison also has direct relevance to additive manufacturing, since the stepped geometry of Model 6 is representative of how a smooth transition would be approximated by a layer-by-layer printing process. The close agreement between Model 7 and Model 1 therefore suggests that if the layer

thickness of the printing process is sufficiently small, the resulting staircase approximation will have a negligible effect on the filter response.
In summary, going three-dimensional is achievable, but adding a dimension does not automatically improve a filter. Changes the constraints that must be managed. Three conditions proved essential across all models: a controlled return current path, well-placed ground planes, and smooth transitions between filter sections. Since none of the models were optimized, these results represent feasibility trends rather than final performance limits, and better performance is likely achievable once the geometry is tuned.

7.2 Future Work

Several extensions of this work would be worth pursuing.
Building and measuring physical prototypes using AME is the natural next step, as simulations can go only so far without experimental confirmation. This would make it possible to evaluate the practical feasibility of the designs and identify discrepancies between the simulated and measured results that arise from fabrication tolerances, material losses, connector effects, and deviations in material properties compared to the ideal values assumed in this study.
A systematic study of manufacturing tolerances would also be of interest, particularly for Model 6 and Model 7 where the filter response is expected to be most sensitive to geometrical deviations. Such a study could investigate how variations in step height, transition angle, and layer thickness affect the S-parameter response and provide guidance on the manufacturing precision required to achieve the intended filter behavior.
Systematic optimization of the geometry is another clear direction, particularly for Model 7 which already performs close to the reference filter. A parametric study of transition angle, length, and ground placement could provide further insight into how response can be improved. For Model 4, varying the vertical height and the internal ground configuration would help determine how the resonant behavior depends on the electrical volume of the structure. For Model 5, further work could investigate how spiral dimensions, ground placement, and conductor spacing affect cutoff frequency and impedance matching.
The design principles identified in this study could also be extended to other filter types and frequency ranges. Applying the same comparative methodology to higher-order Chebyshev low-pass filters, band-pass filters, and other microwave filter topologies would provide a broader understanding of how three-dimensional design techniques can be applied in practical microwave systems.
Future work should also include a broader SWaP-C evaluation. Weight, power handling, manufacturing cost, and process-specific limitations associated with additive manufacturing were outside the scope of this work, but these factors are important to assess the practical suitability of three-dimensional microwave filter structures in compact microwave systems, such as phased-array radar architectures.
Finally, material properties deserve closer attention in future work, especially the frequency-dependent behavior of AME substrates, which this study assumed to be ideal and constant [1, 4]. Accounting for their frequency dependence would provide a

more realistic picture of the expected performance of additively manufactured filter structures in practical applications.

Bibliography

[1] M. Li, Y. Yang, Y. Zhang, F. Iacopi, S. Ram, and J. Nulman, "A fully integrated conductive and dielectric additive manufacturing technology for microwave circuits and antennas," in *Proc. European Microwave Conference (EuMC)*, 2020, pp. 392–395. doi:10.23919/EuMC48046.2021.9338141.

[2] D. M. Pozar, *Microwave Engineering*, 4th ed. Hoboken, NJ, USA: Wiley, 2012.

[3] M. Li, Y. Yang, F. Iacopi, M. Yamada, and J. Nulman, "Compact multilayer bandpass filter using low-temperature additively manufacturing solution," *IEEE Transactions on Electron Devices*, vol. 68, no. 7, pp. 3163–3169, Jul. 2021. doi:10.1109/TED.2021.3072926.

[4] D. Sokol, M. Yamada, and J. Nulman, "Design and performance of additively manufactured in-circuit board planar capacitors," *IEEE Transactions on Electron Devices*, vol. 68, no. 11, pp. 5747–5752, Nov. 2021. doi:10.1109/TED.2021.3117934.

[5] K. Kurokawa, "Power waves and the scattering matrix," *IEEE Transactions on Microwave Theory and Techniques*, vol. 13, no. 2, pp. 194–202, Mar. 1965. doi:10.1109/TMTT.1965.1125964.

A

Appendix 1

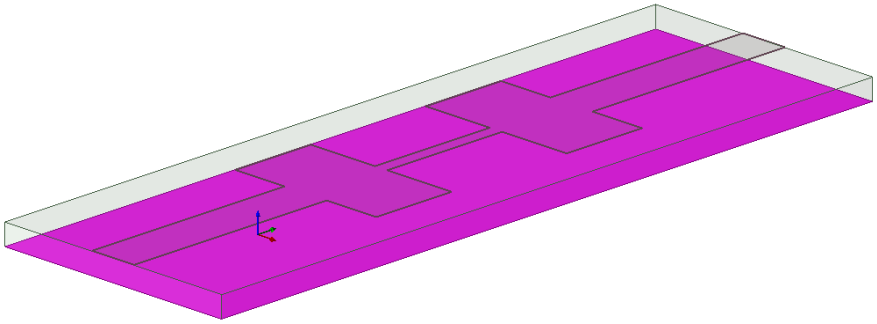

Figure A.1: Model 1 marked ground plane

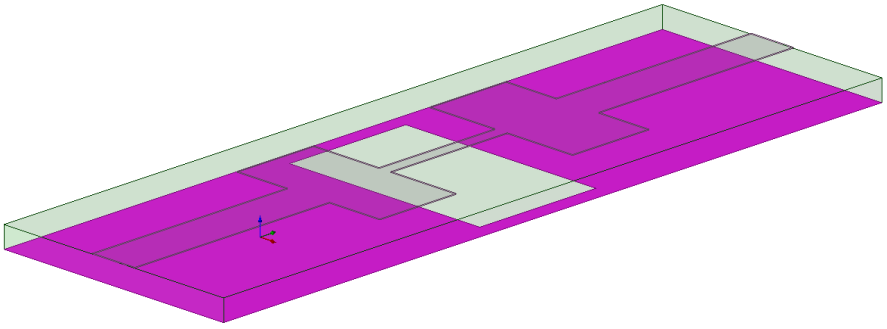

Figure A.2: Model 2 marked ground plane

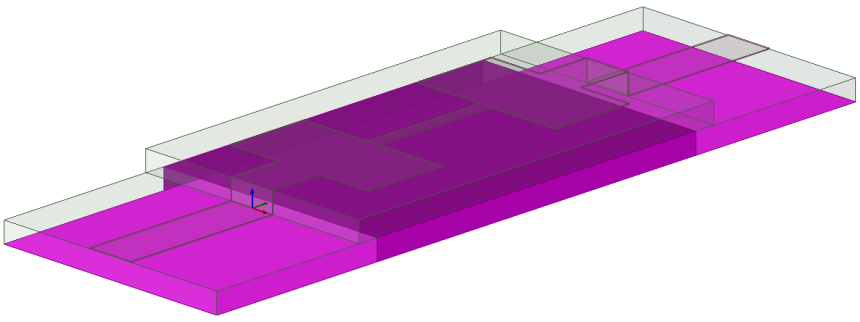

Figure A.3: Model 3 marked ground plane

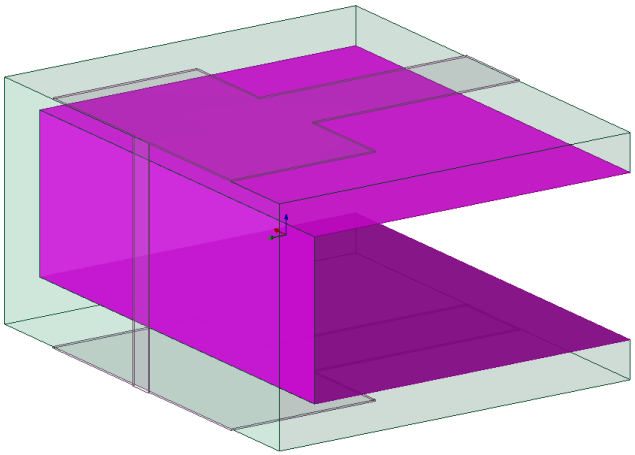

Figure A.4: Model 4 marked ground plane

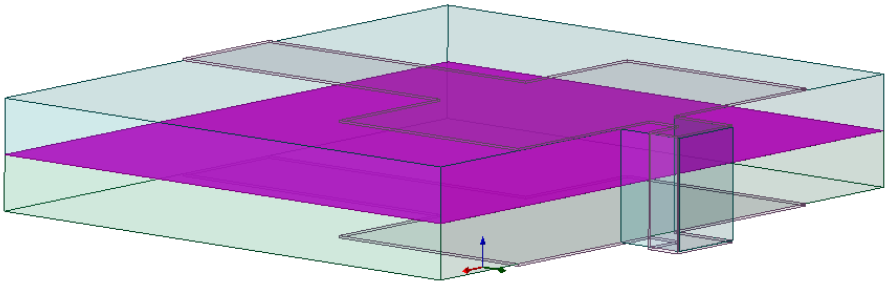

Figure A.5: Model 5 marked ground plane

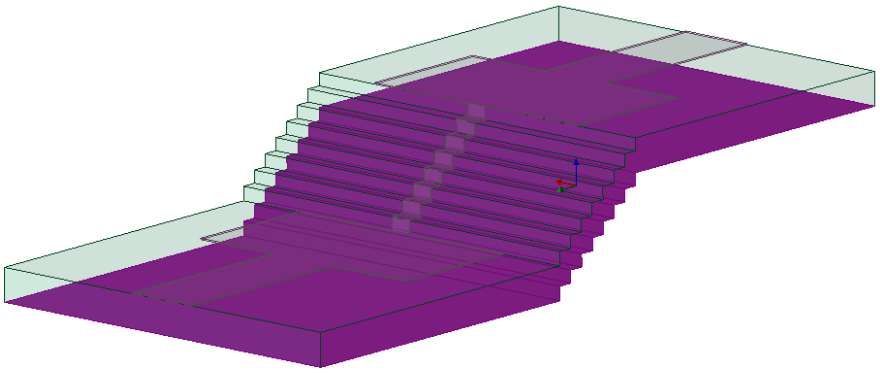

Figure A.6: Model 6 marked ground plane

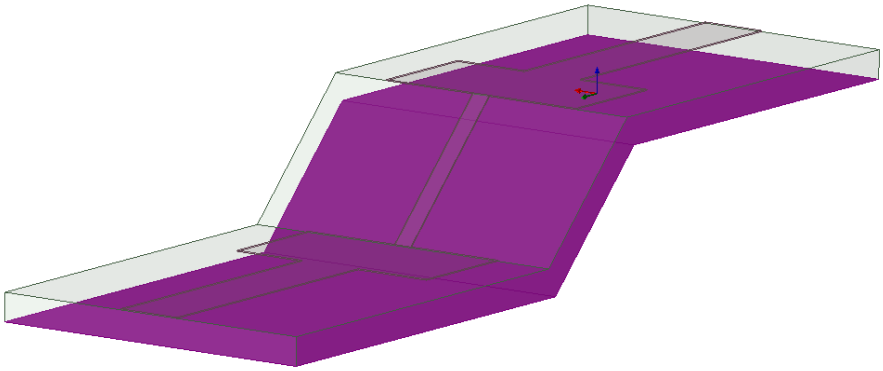

Figure A.7: Model 7 marked ground plane

Department of Microtechnology and Nanoscience
CHALMERS UNIVERSITY OF TECHNOLOGY
Gothenburg, Sweden
www.chalmers.se